

INVERTED ORGANIC SOLAR CELL APPLICATIONS OF
BENZODITHIOPHENE AND BENZOTRIAZOLE BEARING ALTERNATING
COPOLYMERS

A THESIS SUBMITTED TO
THE GRADUATE SCHOOL OF NATURAL AND APPLIED SCIENCES
OF
MIDDLE EAST TECHNICAL UNIVERSITY

BY

EDA BOLAYIR

IN PARTIAL FULFILLMENT OF THE REQUIREMENTS
FOR
THE DEGREE OF MASTER OF SCIENCE
IN
CHEMISTRY

JULY 2018

Approval of the thesis:

**INVERTED ORGANIC SOLAR CELL APPLICATIONS OF
BENZODITHIOPHENE AND BENZOTRIAZOLE BEARING
ALTERNATING COPOLYMERS**

submitted by **EDA BOLAYIR** in partial fulfillment of the requirements for the degree
of **Master of Science in Chemistry Department, Middle East Technical University**
by,

Prof. Dr. Halil Kalıpçılar
Dean, Graduate School of **Natural and Applied Sciences** _____

Prof. Dr. Cihangir Tanyeli
Head of Department, **Chemistry** _____

Prof. Dr. Levent Toppare
Supervisor, **Chemistry Dept., METU** _____

Examining Committee Members:

Prof. Dr. Ali Çırpan
Chemistry Dept., METU _____

Prof. Dr. Levent Toppare
Chemistry Dept., METU _____

Prof. Dr. Yasemin Arslan Udum
Technical Sciences Vocational School, Gazi University _____

Assoc. Prof. Dr. Emren Nalbant Esentürk
Chemistry Dept., METU _____

Assoc. Prof. Dr. İrem Erel Göktepe
Chemistry Dept., METU _____

Date: _____ 16.07.2018 _____

I hereby declare that all information in this document has been obtained and presented in accordance with academic rules and ethical conduct. I also declare that, as required by these rules and conduct, I have fully cited and referenced all material and results that are not original to this work.

Name, Last name :

Signature :

ABSTRACT

INVERTED ORGANIC SOLAR CELL APPLICATIONS OF BENZODITHIOPHENE AND BENZOTRIAZOLE BEARING ALTERNATING COPOLYMERS

BOLAYIR, Eda
MSc., Department of Chemistry
Supervisor : Prof. Dr. Levent Toppare

July 2018, 58 pages

In this thesis, electrochemical, optical and photovoltaic studies of two novel benzodithiophene and 1,2,3-benzotriazole bearing alternating copolymers were investigated. Benzodithiophene which has a strong electron donating ability and planar structure was used as the donor moiety. On the other hand, benzotriazole was used as an acceptor moiety due to its electron deficient nature. In order to determine the effect of π -bridges, thiophene (P1) and selenophene (P2) moieties were incorporated between the donor and acceptor units. Electrochemical studies revealed that both polymers have ambipolar character. Cyclic voltammetry analysis were carried out to calculate HOMO and LUMO energy levels of polymer P1 and P2.

Inverted organic photovoltaic applications of polymers were constructed as following ITO / ZnO / POLYMER:PC₇₁BM / MoO₃ / Ag. The J-V measurements of the photovoltaic devices were performed under the standard AM 1.5G illumination. AFM and TEM techniques were used in order to examine thickness and morphology of the polymer films. As a result of several optimization studies, power conversion efficiencies were achieved as 1.30% for P1 and 1.02% for P2, respectively.

Keywords: Donor, acceptor, π -bridge, inverted organic solar cell, power conversion efficiency

ÖZ

BENZODİTİYOFEN VE BENZOTRIAZOL İÇEREN SIRALI KOPOLİMERLERİN TERS ORGANİK GÜNEŞ GÖZESİ UYGULAMALARI

BOLAYIR, Eda
Yüksek Lisans, Kimya Bölümü
Tez Yöneticisi : Prof. Dr. Levent Toppare

Temmuz 2018, 58 sayfa

Gerçekleştirilen bu tezde, iki yeni benzodityofen ve benzotriazol içeren sıralı kopolimerlerin elektrokimyasal, optiksel ve fotovoltaik çalışmaları araştırılmıştır. Güçlü elektron verme özelliği ve yüzelsel yapısı ile benzodityofen donör olarak kullanılmıştır. Benzotriazol ise elektronca eksik yapısı ile akseptör olarak kullanılmıştır. Buna ek olarak, π köprüsünün etkisini görmek için tiyofen (P1) ve selenofen (P2) üniteleri donör ve akseptör ünitelerinin arasına yerleştirilmiştir. Elektrokimyasal çalışmalar iki polimerin de pozitif ve negatif doplanabildiklerini göstermiştir. Ayrıca, polimerlerin enerji seviyelerini hesaplamak için dönüşümlü voltametri kullanılmıştır.

Ters organik güneş gözesi için ITO / ZnO / POLİMER:PC₇₁BM / MoO₃ / Ag dizilimi kullanılmıştır. Akım Yoğunluğu-Voltaj ölçümleri standart AM 1.5G aydınlatma ile yapılmıştır. Kalınlık ve morfoloji incelemeleri AFM ve TEM ile belirlenmiştir. Yapılan birçok optimizasyon sonucunda, P1 ve P2 polimerlerinin güç dönüşüm verimlilikleri sırasıyla %1.30 ve %1.02 olarak hesaplanmıştır.

Anahtar Kelimeler: Donör, akseptör, π köprüsü, ters organik güneş gözesi, güç dönüşüm verimliliği

To my lovely family...

ACKNOWLEDGMENTS

I would like to thank my supervisor Prof. Dr. Levent Toppare for his endless support, patience and encouragement during my time as his student. He showed me how to solve problems and deal with them in academic life. His immense knowledge and experiences influenced my perspective about science deeply. It was a great honor to work with him.

I would like to express my gratitude to Prof. Dr. Ali Çırpan for his helpful comments and suggestions on my research. He was always there when I needed him.

I would like to acknowledge Prof. Dr. Yasemin Udum Arslan, Assoc. Prof. Dr. Emren Nalbant Esentürk and Assoc. Prof. Dr. İrem Erel Göktepe as the second reader of this thesis, and I am thankful to their invaluable comments.

I am very grateful to Şevki Can Cevher for the syntheses of the polymers.

I must also acknowledge Dr. Şerife Özdemir Hacıoğlu for her contributions on electrochemical characterizations.

I would like to thank Dr. Gönül Hızalan Özsoy for her invaluable feedbacks on my research which enlightened my point of view. Her endless support, encouragement and patience made me to do my best. She was always there for me as a mentor, friend and sister whenever I needed her. I have admired her working discipline during my master study and I hope I would be as good as she is one day.

My sincere thanks also go to my dearest friends Seza Göker, Mert Can Erer, Ecem Aydan, Hande Özel and Eda Alemdar who were always ready to help and motivate me. Their friendships were irreplaceable. It would be a very lonely and boring lab if I would not have them.

I thank my sweetest friends Begüm Avcı and Merve Nur Güven for being my besties since undergraduate years. I laughed and cried with those two. I have always

remembered them even we could not have any chance to see each others. It is an amazing feeling to know that someones will always love you unconditionally.

My warmest thank goes to my beloved Ece Büber who was my friend, companion and confidant. She was my sister that I have never met until I started the university. She cared and understood me in every point of my life. I am so lucky to have you my Bieber. There are so many memories that we had and so many that we will. I ensure you with no doubt you will be in my heart and life forever. Team Bolber never lets each others down.

Last but not least, I would like to thank my magnificent family to whom i owe my everything. I have no words to describe my mother's love, care and support. Her hugs were my consolation and her words were my lead. I am thankful to my sweet father for his understanding and patience. I owe a lot to my precious brother Ata Bolayır for his limitless support and encouragement. I can not imagine a life without him. He is my brother, friend and second father that always watching my back.

This work is partially supported by Scientific and Technological Research Council of Turkey (TÜBİTAK) (Project No: 155M036).

TABLE OF CONTENTS

ABSTRACT	v
ÖZ.....	vii
ACKNOWLEDGMENTS.....	ix
TABLE OF CONTENTS.....	xi
LIST OF TABLES.....	xiv
LIST OF FIGURES	xv
CHAPTERS	
1. INTRODUCTION.....	1
1.1 Conducting Polymers	1
1.2 Applications of Conducting Polymers	3
1.2.1 Electrochromic Devices	3
1.2.2 Organic Light Emitting Diodes (OLEDs).....	5
1.2.2.1 Luminescence	5
1.2.2.1.1 Photoluminescence	6
1.2.2.1.2 Electroluminescence	8
1.2.2.2 Working Principle of OLEDs	9
1.2.2.3 Device Structure of OLEDs.....	10
1.2.3 Organic Photovoltaics.....	10
1.2.3.1 Bulk Heterojunction Basis in OPVs.....	13
1.2.3.2 Working Principle of IOSCs.....	14
1.2.3.3 Device Design of IOSCs.....	16
1.2.3.3.1 Cathode	17

1.2.3.3.2	Electron Transport Layer (ETL)	17
1.2.3.3.2.1	ZnO	17
1.2.3.3.3	Active Layer	18
1.2.3.3.4	Hole Transport Layer (HTL)	20
1.2.3.3.4.1	MoO ₃	20
1.2.3.3.5	Anode	21
1.3	Organic Photovoltaic Parameters.....	21
1.3.1	Short Circuit Current Density (J_{sc}).....	23
1.3.2	Open Circuit Voltage (V_{oc})	23
1.3.3	Fill Factor (FF)	23
1.3.4	Power Conversion Efficiency (PCE).....	24
1.3.5	External Quantum Efficiency (EQE).....	24
1.4	Morphology Control in the BHJ Active Layer	25
1.4.1	D-A Blend Ratio	25
1.4.2	Solvent Effect	25
1.4.3	Thermal Annealing	26
1.4.4	Solvent Annealing.....	27
1.4.5	Processing Additive	27
1.5	Aim of the Study	27
2.	EXPERIMENTAL.....	31
2.1	Materials	31
2.2	Equipments	31
2.3	Synthesis of Polymers	32
2.4	Electrochemical Studies	32
2.5	Optical Studies	33

2.6 Photovoltaic Studies.....	33
2.6.1 Device Fabrication of IOSCs	33
2.6.1.1 ITO Cleaning	33
2.6.1.2 Electron Transport Layer (ETL)	34
2.6.1.3 Active Layer.....	34
2.6.1.4 Thermal Evaporation	34
2.6.2 Characterization of IOSCs	35
3. RESULTS AND DISCUSSION	37
3.1 Electrochemical Studies	37
3.2 Optical Studies	39
3.3 Photovoltaic Studies	40
4. CONCLUSION	47
REFERENCES.....	49
APPENDICES	
A. Energy Level Diagram of Devices	55
B. Molar Absorption Coefficients of P1 and P2	57

LIST OF TABLES

TABLES

Table 3.1 Summary of the electrochemical studies	39
Table 3.2 Summary of the optical studies	40
Table 3.3 Summary of the photovoltaic studies of P1	42
Table 3.4 Summary of the photovoltaic studies of P2	42

LIST OF FIGURES

FIGURES

Figure 1.1: The structure of given polymers (a) polyacetylene, (b) poly(p-phenylenevinylene), (c) polyfuran, (d) poly(3-hexylthiophene-2,5-diyl).....	2
Figure 1.2: (a) Electrochromic Device, (b) Organic Light Emitting Diodes, (c) Organic Photovoltaic	3
Figure 1.3: Schematic representation of electrochromic device construction	4
Figure 1.4: Spin orientations in singlet ground and excited states and triplet excited state	7
Figure 1.5: Jablonski Diagram	7
Figure 1.6: Electroluminescence of fluorescent and phosphorescent molecules	8
Figure 1.7: Operation of an OLED	9
Figure 1.8: Device Design of OLED	10
Figure 1.9: Device structure of (a) conventional (b) inverted organic solar cell	12
Figure 1.10: Device structure of (a) bilayer (b) bulk heterojunction organic solar cell	14
Figure 1.11: Energy diagram of organic semiconductor.....	15
Figure 1.12: Operation principle of inverted organic solar cell	16
Figure 1.13: Device Structure of IOSC.....	16
Figure 1.14: Molecular orbital hybridization of energy levels	20
Figure 1.15: The J-V curve of solar cell under illumination	22
Figure 1.16: AM 1.5G standardization	22
Figure 1.17: TEM images of thin films spin cast from (a) CF, (b) CB, (c) DCB	26
Figure 1.18: Scheme of D-A blend aggregation (a) without additive, (b) with additive	28

Figure 1.19: Chemical structures of P1 and P2, respectively	29
Figure 3.1: Cyclic Voltammograms of the P1 and P2, respectively in 0.1 M TBAPF ₆ /ACN.....	38
Figure 3.2: Absorption spectra of P1 and P2, respectively.....	40
Figure 3.3: J-V curve of IOSCs based on P1:PC ₇₁ BM blend ratios	41
Figure 3.4: J-V curve of IOSCs based on P2:PC ₇₁ BM blend ratios	41
Figure 3.5: J-V curves of P1 in different additives	43
Figure 3.6: J-V curves of P2 in different additives	44
Figure 3.7: TEM images of (a) P1:PC ₇₁ BM (1 μm), (b) P1: PC ₇₁ BM +3% DPE (1 μm), (c) P2: PC ₇₁ BM (500 nm), (d) P2: PC ₇₁ BM +3% CN (500 nm).....	45
Figure 3.8: IPCE curves of the best performance solar cells of P1 and P2	45

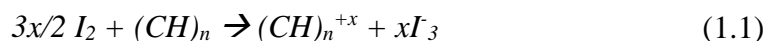
CHAPTER 1

INTRODUCTION

1.1 Conducting Polymers

In the early 1970s, Alan G. McDiarmid and Alan J. Heeger, in USA, were synthesized the electrically conductive polymeric sulfur nitride $(SN)_x$ from S_2N_2 crystals. Electrical conductivity of polythiazyl was measured as $2.5 \times 10^3 \text{ Scm}^{-1}$ at room temperature and its conductivity enhanced almost 225 times more with lowering temperature (10 K) in which achieved superconductivity at 0.26 K [1][2].

At the same time in Japan, silvery film of polyacetylene (PA) was prepared by Hideki Shirakawa and his students using concentrated Ziegler-Natta catalyst. After Natta et al. who was the first group to synthesize linear, regular structure, high molecular weight black powder polyacetylene, Shirakawa's method became widely used procedure for the polymerization of acetylene since unlike Natta's polymerization, Shirakawa's polyacetylene was soluble and relatively stable [3]. However, even though its metallic appearance, synthesized polyacetylene was not a conductor. In 1977, McDiarmid, Heeger and Shirakawa discovered that conductivity of polyacetylene films could be increased by 10^9 times more when they are exposed to chlorine, bromine or iodine vapor. Thus, upon doping, un-doped insulator polymers can be conductive like metals.



The oxidation of polymer backbone by iodine vapor generates hole, an electron vacancy, which provides charge mobility on the polymer chains thus conductivity. The treatment with halogen vapor was then called ‘doping’.

The highest conductivity of PA was determined as 38 Scm^{-1} at room temperature with I_2 vapor treatment [4]. After all these investigations, these three scientists were awarded by Nobel Prize in Chemistry in 2000 for the ‘discovery and development of electrically conductive polymers’.

Conducting polymers should possess two major properties to conduct electricity;

- *Conjugation* that is an alternating single and double bond which provides electron delocalization in the polymer backbone thus conductivity.
- *Being dopable* which enables electron or hole injection into the polymer backbone thus charge mobility.

After 2000, extensive research efforts have been devoted on synthesis of conducting polymers due to their advantages over the inorganic materials such as light weight, low cost, simple device fabrication, flexibility, solution processability and tunability on chemical structure [5][6].

Over the last two decades, new conducting polymers with higher solubility and stability have been found. Figure 1.1 illustrates some examples from the literature.

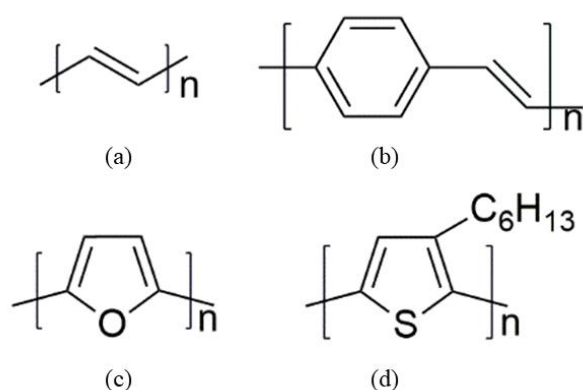


Figure 1.1: The structure of given polymers (a) polyacetylene, (b) poly(p-phenylenevinylene), (c) polyfuran, (d) poly(3-hexylthiophene)

1.2 Applications of Conducting Polymers

Conducting polymers have been used in organic photovoltaics (OPVs), organic light emitting diodes (OLEDs), organic field effect transistors (OFETs) and electrochromic devices (ECDs) as active layer materials due to their excellent features [7]. Some examples are given in Figure 1.2.

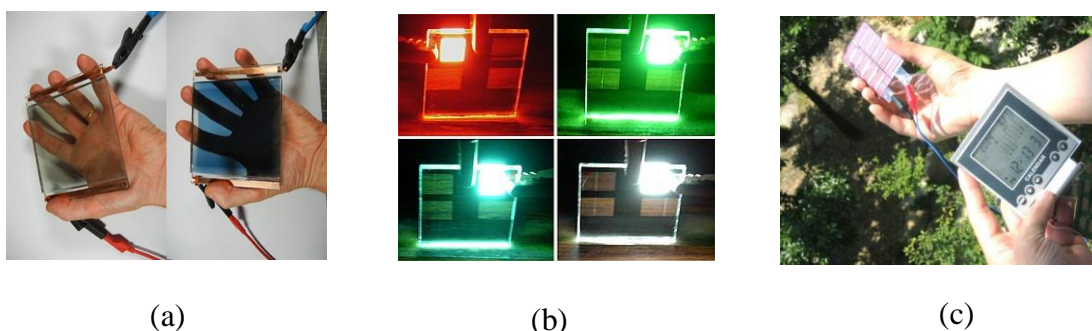


Figure 1.2: (a) Electrochromic Device, (b) Organic Light Emitting Diodes, (c) Organic Photovoltaic

1.2.1 Electrochromic Devices

Electrochromism is a reversible color change of material upon applied potential or electrical current. These optical property changes occur due to the formation of different absorption bands during electrochemical oxidation and reduction processes. Upon from the inorganic materials, conducting polymers exhibit great features such as long term stability, high coloration efficiency, improvable short switching time, high optical contrast, long optical memory and multicolor characteristics [8].

When conducting polymer is oxidized (p-doped) via applying a potential, an electron is removed from its valence band and radical cation that is polaron charge carrier is produced. Further oxidation in polymer chain creates bipolaron charge carrier which is basically dication and its formation can be observed in absorption spectrum in which

a decrease in π - π^* absorption is followed by formation of a new band between 700-1000 nm. Afterwards, reduction process is carried out for reversible redox reactions by gaining electron into conducting polymer chain to obtain un-doped neutral form [9][10].

- *Optical contrast* is a percent transmittance change of the thin film at the highest absorption wavelength of the polymer.
- *Coloration efficiency* is amount of charge which induces optical change in electrochromic polymer film.
- *Optical memory* is the time period that electrochromic device sustains at one color.
- *Switching time* is time that passed from changing from one color to another or from one color to transparent.
- *Device stability* is the cyclic switching performance of electrochromic device without degradation. Note that stability of the polymer thin film is negatively affected by applied high potential which should be considered carefully for commercialization process.

Electrochromic device construction is depicted in Figure 1.3. ITO glasses which serves as working electrodes are spray coated with anodically and cathodically colored electrochromic polymers. Gel electrolyte in micrometer scale is used in order to sandwich the two electrodes. Then, appropriate voltages are applied to observed color change via redox reactions in the polymer chains [11].

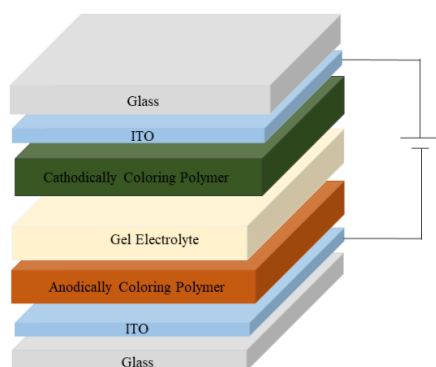


Figure 1.3: Schematic representation of electrochromic device construction

The main application areas of electrochromic devices are rear-view mirrors, smart windows and displays.

1.2.2 Organic Light Emitting Diodes (OLEDs)

Organic light emitting diode (OLED) is a solid state electronic device in which the emissive layer (EML) is a thin film of organic compound that emits light in response to electric current. OLEDs have gained great interest in display technology over the past few decades such as television and phone screens and computer monitors because they are lighter, thinner and more flexible than their counterparts.

History of OLEDs can be ordered as given;

- Andre Bernanos (1950), Electroluminescence in organic material that is acridine orange
- Martin Pope (1960), Development of ohmic electrode and DC electroluminescence on one crystal of anthracene [12]
- Ching W. Tang and Stephan V. Slyke (1987), First OLED applications via using Alq₃ (tris(8-quinolinolato)-aluminium(III)) at Eastman Kodak company [13]
- Richard Friend (1990), Single layer OLED by using highly fluorescent conjugated polymer poly(p-phenylene vinylene) (PPV) [14]

1.2.2.1 Luminescence

Nature is surrounded by a number of types of energy which are converted to each other continuously by the fact that 'Energy can exchange between forms, but it is never destroyed or created.'. There are many types of energy and light is one of them. However, in order to obtain light, another form of energy has to be supplied. This can be carried out with two common ways that are incandescence and luminescence.

Incandescence could be simply defined as generation of light from a hot body outcome of temperature. Tungsten filament bulb or electric stove's heater starts to glow when it gets hot and its brightness begins to decrease when it is getting cold because of incandescence. The biggest example of incandescence is the sun.

Luminescence which is also defined as cool light is the emission of light due to movement of electrons from higher energy state to lower energy state. There are plenty of luminescence types including photoluminescence, electroluminescence, chemiluminescence, bioluminescence. Photoluminescence and electroluminescence methods will be discussed.

1.2.2.1.1 Photoluminescence (PL)

When a molecule absorbs sufficient light energy (photon), it becomes excited which means electrons move to a higher energy state and stay that energy level for a short time ($10^{-4} - 10^{-8}$ s). Then, energy is released by the movement of electrons to the ground state that is called as relaxation. If relaxation is radiative, this phenomenon is called photoluminescence. Emission wavelength is longer than absorption wavelength ($E_{\text{abs}} > E_{\text{em}}$) due to energy loss. Photoluminescence has two main sub-groups that are fluorescence and phosphorescence depending on excited state character.

According to Pauli exclusion principle, no two electrons in an atom can possess the same four quantum numbers. Thus, an orbital is occupied by only two electrons with opposed spin states to require the proposed restriction. In this condition, the spins are said to be paired and show no net magnetic field (diamagnetic). On the other hand, free radicals which have unpaired electrons are affected by magnetic field (paramagnetic).

As shown in Figure 1.4, upon from excitation singlet and triplet excited states are obtained. In excited singlet state, spins of the two electrons are paired. In triplet excited state, spins of the two electrons have become unpaired. Average lifetime of triplet

excited state is around 10^{-4} s to several seconds compared with an average lifetime of singlet excited state that is approximately 10^{-8} s. Although triplet excited state has relatively longer lifetime than singlet excited state, it is less probable event to observe singlet to triplet transition which involves a change in electronic state [15].

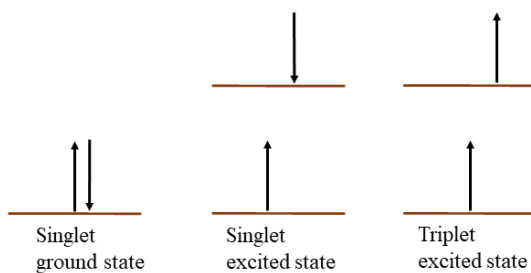


Figure 1.4: Spin orientations in singlet ground and excited states and triplet excited state

Fluorescence and phosphorescence occurrences consisting of energy levels in Jablonski diagram are depicted as Figure 1.5.

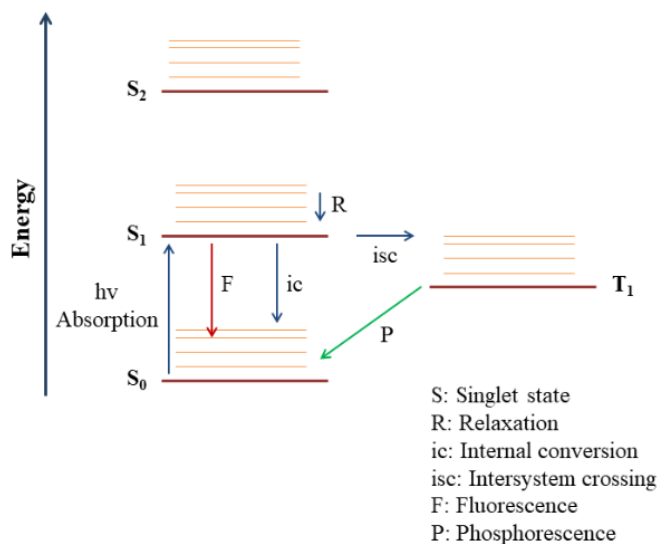


Figure 1.5: Jablonski Diagram

1.2.2.1.2 Electroluminescence (EL)

Electroluminescence is a phenomenon in which luminescence is observed due to externally applied voltage. Injected charge carriers that are electrons and holes combine and radiate in emissive layer. Excitons (electron and hole pair) are electrically neutral and have four different spin combinations. According to their total spin numbers, excitons are called as singlet or triplet excitons. If the total spin of exciton is zero, singlet exciton is obtained. For triplet exciton production total spin number must be one. Upon from electrical current excitation, 1:3 ratio for singlet to triplet exciton production is achieved. As depicted in Figure 1.6, from 100% exciton efficiency in EL, only 25% of it is singlet excitons which give fluorescence emission. The rest of the 75% belongs to triplet excitons with phosphorescence emission. Thus, electroluminescence of phosphorescent molecule based devices results in higher efficiency due to collect triplet excitons.

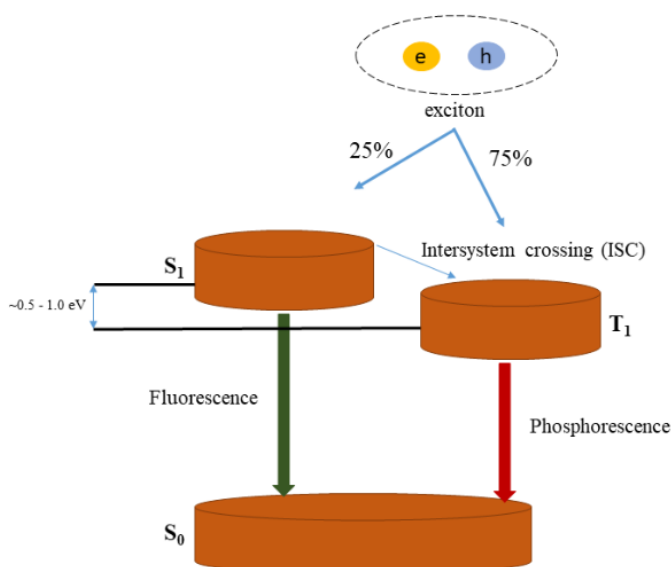


Figure 1.6: Electroluminescence of fluorescent and phosphorescent molecules

1.2.2.2 Working Principle of OLEDs

When an external potential is applied between the electrodes, electrons from low work function (WF) metal cathode and holes from high WF, transparent and conductive anode are injected into LUMO and HOMO energy levels of organic materials, respectively. Due to coulombic attraction, electrons and holes are combined and produce excitons in the emissive layer which gives radiative decay with visible frequency at the end. Figure 1.7 shows schematic representation of working principle of typical OLED.

Hole and electron transport layers with proper energy levels are used in order to make charge carrier transportation easier. When PEDOT:PSS and PVK are good candidates for hole transport layer, LiF is generally used for electron transport layer. For the emissive layer, small molecules, oligomers and polymers are mainly preferred.

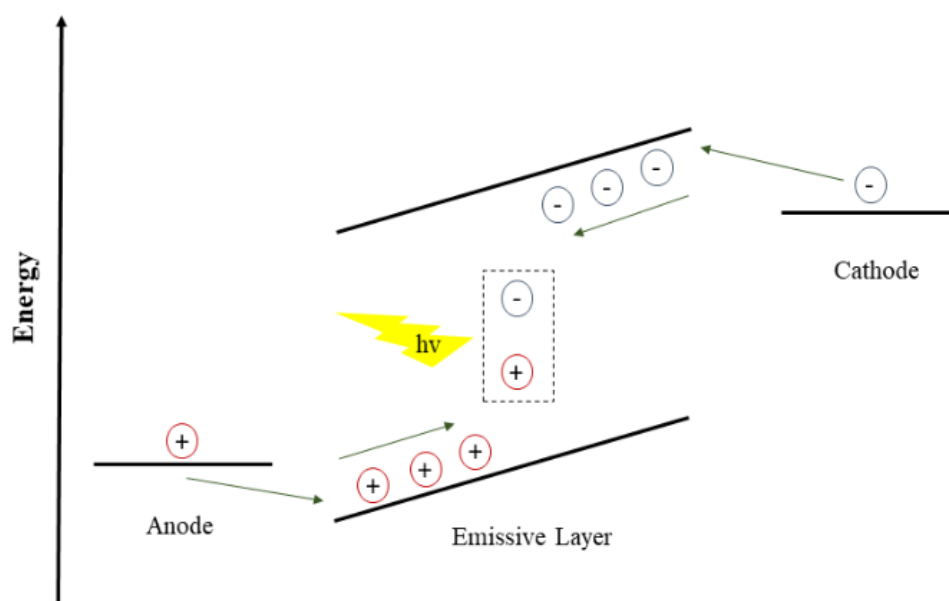


Figure 1.7: Operation of an OLED

1.2.2.3 Device Structure of OLEDs

The device architecture of OLED is represented in Figure 1.8.

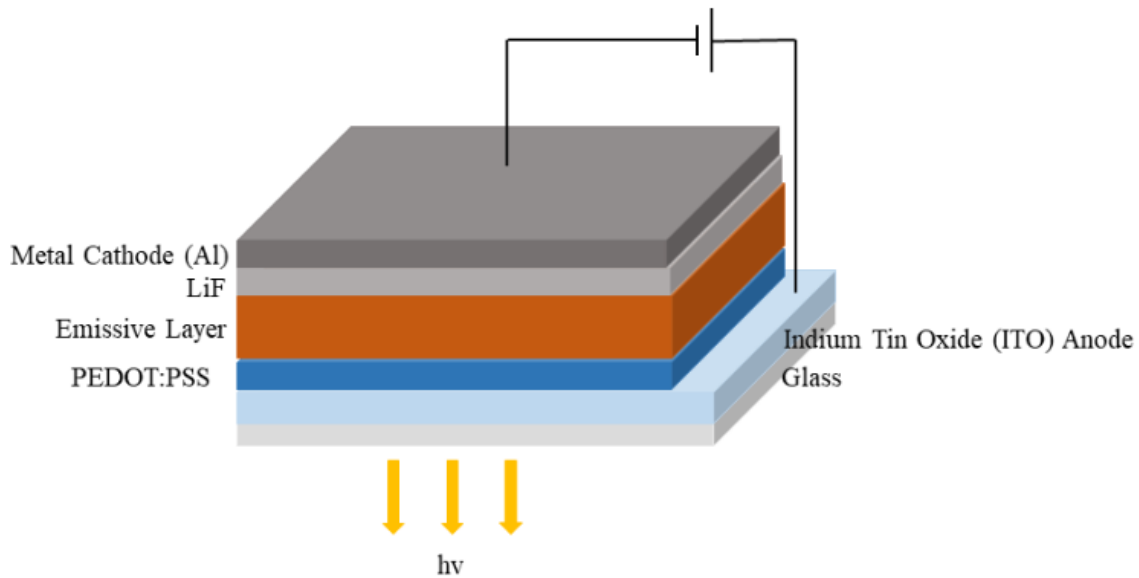


Figure 1.8: Device Design of OLED

1.2.3 Organic Photovoltaics (OPVs)

The currently used fossil fuel energy sources have unignorable consequences on economical and environmental issues. These sources are in limited reserves and do not have desired capacity to supply all the energy requirements. Therefore, renewable energy has gained great interest to provide natural and unlimited sources for energy production and eliminates the stated problems on environmental and economical issues. Upon from all the renewable energy sources, solar energy is the most promising one to meet all the world's growing energy demand. Solar cells which convert sun light into electricity is one of the way to harvest solar energy. Inorganic solar cells based on crystalline silicon, cadmium telluride etc. dominate the photovoltaic

technology due to their relatively high power conversion efficiencies of around 15-20%. However, their high production cost and environmental issues promote research efforts to find alternative approaches. Organic solar cells on the other hand hold promise because of their low cost, light weight, flexibility and tunability in chemical structures as well as being environmentally friendly. Despite the fact that these advantages of organic solar cells, their efficiencies and stabilities are much lower than their inorganic counterparts. Therefore, extensive research methods have been investigated to improve the device performance of organic solar cells.

The first successful organic photovoltaic device was reported by Tang in 1986. The proposed device structure was different from the previous conventional single layer devices in which organic material was sandwiched between the two dissimilar electrodes. Therefore, difference in work functions of electrodes derived the built-in potential. In Tang's experiment, the bilayer device construction was designed by using p-type copper phthalocyanine (CuPc) and n-type perylene tetracarboxylic derivative (PV). Organic layers were coated on ITO-glass via vacuum evaporation. Then, opaque Ag metal was evaporated on top of the CuPC-PV layer as the cathode. Power conversion efficiency of about 1% with a fill factor of 65% was obtained. High fill factor value was achieved in the bilayer device structure by decreasing the series resistance [16].

In 1993, ultrafast electron transfer from conjugated polymer poly(2-methoxy-5-(2-ethylhexyloxy))-1,4-phenylenevinylene (MEH-PPV) to fullerene (C_{60}) was discovered by Heeger and Wudl group which opened a new era for the use of conjugated polymers as donors and fullerene derivatives as acceptors [17]. Today, power conversion efficiency of polymer-fullerene based (D-A type) organic solar cells found over 11% [18]. This number is higher (over 12%) for small molecule-nonfullerene based organic solar cells [19]. Recently, fluorinated PBDB-T and ITIC based organic photovoltaic devices showed efficiency of 13.1% [20].

Organic photovoltaics based on conventional device structures have some

disadvantages in terms of low stability and high production cost. In order to eliminate these problems, inverted device structures have been developed.

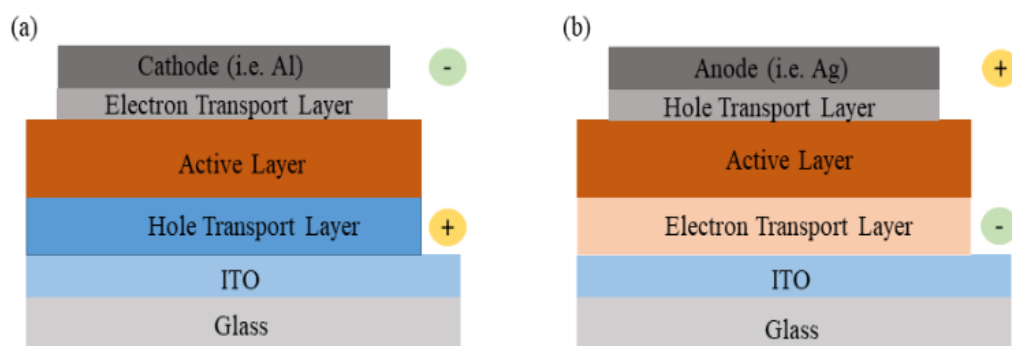


Figure 1.9: Device structure of (a) conventional (b) inverted organic solar cell

Figure 1.9 illustrates conventional and inverted organic solar cell architectures. In conventional device, organic active layer is sandwiched between the high work function transparent conducting indium tin oxide (ITO) anode and low work function metal cathode such as aluminum (Al) calcium (Ca) and barium (Ba). Typically, poly(3,4-ethylenedioxythiophene):poly(styrenesulfonate) (PEDOT:PSS) is used as the hole transport layer to smooth the ITO electrode surface and provide better charge carrier (hole) collection at the anode. However, acidic nature of PEDOT:PSS especially at elevated temperature and humidity can etch the ITO surface over time [21]. Moreover, large microstructural and electrical inhomogeneities of PEDOT:PSS layer causes variations in film morphology and electrical conductive properties which deteriorates charge transportation and leads to poor device performance [22]. Furthermore, metal electrode deposition via vacuum evaporation is an expensive technique and not appropriate for the large-scale roll-to-roll process.

In inverted device structure, ITO acts as the cathode and high work function metals are used as the anodes. Thus, direction of the charge collection is reversed. PEDOT:PSS layer is removed from the top of the ITO surface in order to avoid stated etching and inhomogeneity problems. Also, air-sensitive Al is replaced with air-stable silver (Ag) or gold (Au) for anode electrode stability against oxidation by air and humidity.

Moreover, usage of these metals makes printing technologies possible for metal electrode deposition instead of using energy consuming thermal deposition technique which enables roll-to-roll production of inverted organic solar cells [23].

In this thesis study, inverted organic solar cell will be examined in detail.

1.2.3.1 Bulk Heterojunction Basis in OPVs

For the high performance organic photovoltaics, several requirements should be fulfilled such as efficient absorption of light by donor, excellent charge carrier generation, transportation and collection. When an organic semiconductor is photoexcited, it creates excitons instead of free charge carriers like inorganic solar cells. Low dielectric constant and high exciton binding energy values of organic semiconductors prevents exciton dissociation at room temperature but in order to create a photovoltaic effect this process must occur. Such dissociation can be achieved by heterojunction of two organic semiconductors with proper electron affinity differences which acts as an additional field [24].

The first successful heterojunction formation was proposed by Tang in 1986 as a bilayer solar cell [16]. In bilayer device architecture, electron donor (organic semiconductor) and electron acceptor (fullerene and nonfullerene) are sandwiched between the anode and cathode. This work possessed main steps of efficient photovoltaic device that are absorption of light by the donor-exciton formation, exciton diffusion and dissociation at D-A interface and transportation of separated charge carriers at corresponding electrodes. However, further studies have revealed that this device structure leads to small D-A interfacial areas and limited effective charge separation due to the short exciton diffusion length (less than 10 nm). Therefore, power conversion efficiency of bilayer device is low [25].

In order to obtain large D-A interfacial area, the bulk heterojunction (BHJ) structure as depicted in Figure 1.10 was proposed by blending donor and acceptor materials forming an interpenetrating network by controlling the phase separation in the bulk.

In BHJ device structure, the large D-A interfaces provide enhanced charge separation. Due to interpenetrating network, efficient charge transportation and collection are achieved. Through controlling the morphology of the phase separation, higher power conversion efficiency values can be obtained [26][27].

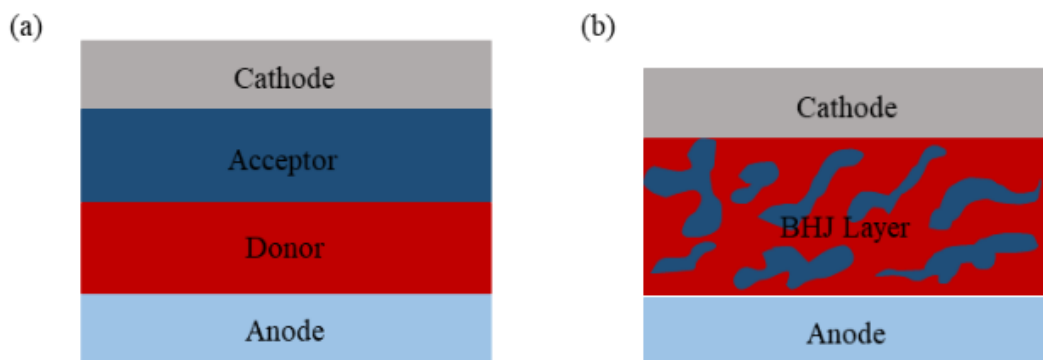


Figure 1.10: Device structure of (a) bilayer (b) bulk heterojunction organic solar cell

1.2.3.2 Working Principles of Inverted Organic Solar Cells (IOSCs)

For an efficient light absorption, band gap of the organic semiconductor plays an important role since absorption range in solar spectrum depends on energy difference between the valence (HOMO) and conduction (LUMO) bands of semiconductor. If this difference is small, absorption to longer wavelengths is achieved that induces higher number of exciton generation. Organic semiconductors generally have larger band gaps around 2 eV which leads to absorption up to 700 nm in solar spectrum. However, for a sufficient absorption, broad range of solar spectrum should be absorbed. Therefore, organic materials with narrow band gaps have been devoted to synthesize. Figure 1.11 illustrates energy diagram of organic semiconductors.

When light is absorbed mainly by the donor (p-type material), electron of donor material is excited from HOMO energy level to LUMO energy level which creates exciton. This coulombically bound electron-hole pair moves through the donor

material and dissociate at the donor-acceptor interface since chemical potential difference of the two organic materials provides sufficient energy to separate the generated exciton forming free charge carriers. Note that in order to enhance the exciton dissociation, large donor-acceptor interfacial area is needed. Then, electrons and holes are transported to the corresponding electrodes to generate photocurrent [28].

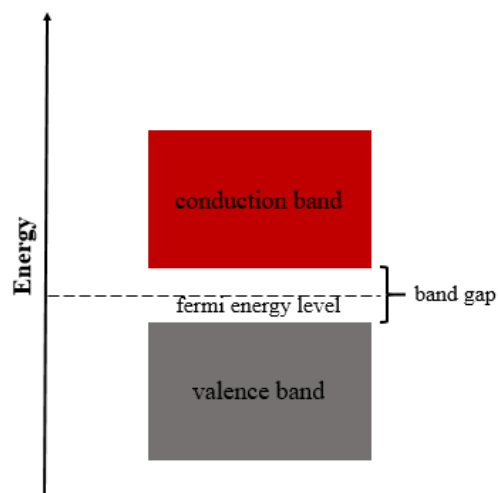


Figure 1.11 Energy diagram of organic semiconductor

Then, free charge carriers are extracted towards corresponding electrodes where electrons go to cathode and holes to anode. In OPVs, ohmic contact which is the junction between the metal and organic semiconductor should be ensured to increase charge extraction. This can be achieved by proper selection of anode and cathode materials. As represented in Figure 1.12, in order to obtain a better charge carrier collection, suitable energy level alignment must be done.

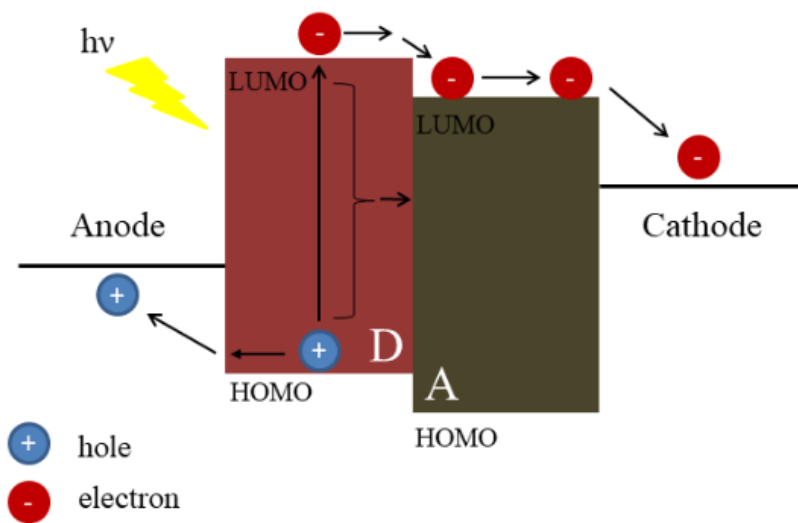


Figure 1.12: Operation principle of inverted organic solar cell

1.2.3.3 Device Design of IOSCs

Device architecture of inverted organic solar cell is shown in Figure 1.12. It consists of active layer as a blend of donor and acceptor materials, hole and electron transport layers and anode and cathode electrodes.

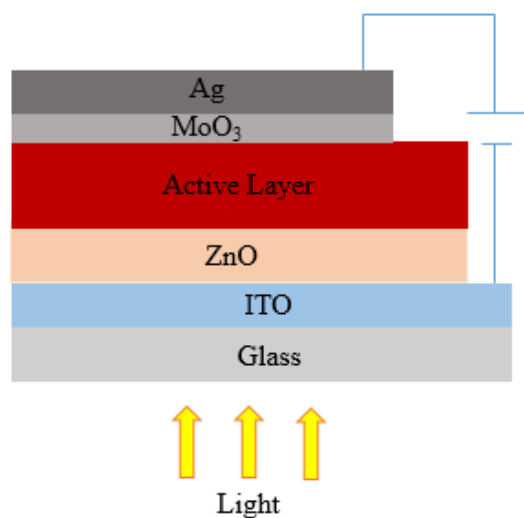


Figure 1.13: Device Structure of IOSC

1.2.3.3.1 Cathode

ITO and fluorine-doped tin oxide (FTO) are generally used as the cathode in IOSCs due to their high conductivity, high work function, good transparency, non-toxicity and good film forming ability in order to possess good contact with adjacent organic layers [29].

1.2.3.3.2 Electron Transport Layer (ETL)

In inverted organic solar cells, electron transport layer is inserted between the active layer and cathode to provide electron extraction and transportation as well as blocking the reverse flow of holes to the cathode. For a better OPV performance, selected ETL should have a good electron transport property and transparency. There are some materials that comply with these requirements such as transition metal oxides (like ZnO, TiO_x), alkali metal compounds and ultra thin layers. In this work, attention will be focused on ZnO due to its good electronic matching ability with the LUMO of most of the organic materials.

1.2.3.3.2.1 ZnO

Zinc oxide is the most representative ETL due to its good transparency, high electron mobility, well hole blocking ability, low production cost and non-toxicity. ZnO is used as the n-type material in solar cells. Its HOMO and LUMO energy levels are -7.6 eV and -4.3 eV, respectively. These energy levels provide proper matching with the HOMO and LUMO energy levels of commonly used donors and acceptors thus decreases significant energy loss.

ZnO deposition can be performed by means of several techniques such as sol-gel, atomic layer deposition (ALD), nanoparticle deposition and spray-coating. In terms of production cost and simplicity, sol-gel method is generally preferred. In 2006, White

et al fabricated an inverted organic solar cell using solution processed ZnO prepared with zinc acetate in 2-methoxyethanol and ethanolamine as an electron transport layer. Device structure of ITO/ZnO/P3HT:PC₆₁BM/Ag showed comparable power conversion efficiency with an increased short circuit current density (J_{sc}). This enhancement is explained by efficient light trapping mechanism: light is scattered by ZnO layer and reflected back by the Ag metal electrode in many directions thus absorbed light can stay in the active layer for a longer time caused enhanced light absorption [30].

Overall performance of the device is strongly depends on morphology of the ZnO layer. Therefore, all the deposition parameters should be taken into account for the selected method. In the sol-gel technique, annealing process plays an important role. Researches have been proven that slow annealing rate gives higher fill factor (FF) with improved morphology due to better crystallization. Moreover, annealing temperature should also be considered as a key factor. ZnO films at different temperatures were tested and characterized by Raman measurements. Results have shown that 150 °C annealed thin film had better crystallization, electron mobility and electron transportation. Thus, both annealing rate and temperature should be taken into consideration for optimum ZnO crystallization [31].

Furthermore, effect of ZnO film thickness on morphology have been studied. Hu et al demonstrated ZnO thickness had a great impact on crystal structure hence on electrical properties. In particular, they confirmed that increase in ZnO film thickness (up to 100 nm) with proper surface roughness was desired for device performance (PCE of 1.60% for 40 nm ZnO, 2.93% for 80 nm) while thicker film layers caused decrease in efficiency [32].

1.2.3.3.3 Active Layer

Active layer of BHJ inverted organic solar cell is composed of electron donor (p-type) and electron acceptor (n-type) materials. Fullerene derivatives such as PC₆₁BM and

PC₇₁BM are used as electron acceptors in OPVs due to their small reorganization energies, high electron mobilities, triply degenerate low lying LUMO energy levels and improved electron transport abilities [33]. However, fullerene-based acceptors have some limitations like weak absorption in the abundant region of the solar spectrum which results in insufficient photocurrent, morphological instability, high production cost. Therefore, non-fullerene derivatives such as ITIC and IEIC have been developed to eliminate these problems while retaining the advantageous properties of fullerenes [34].

After the discovery of electrically conducting polymers in 1977, conjugated polymers as electron donors in organic photovoltaic applications have gained great attention. In order to harvest the sunlight efficiently, narrow band gap polymers with better optical and electronic properties were synthesized. However, proper device operation requires low lying HOMO energy level to increase the V_{oc} and high lying LUMO energy level (higher LUMO of the acceptor) for efficient charge dissociation at the donor-acceptor bulk heterojunction. Introducing the donor (D) and acceptor (A) monomers together in the polymer backbone is the most promising method for tailoring the band gap of conducting polymers. Upon this strategy, compressed band gap is achieved by molecular orbital hybridization and intramolecular charge transfer of interacted alternating electron-rich donors and electron-poor acceptors [35]. As depicted in Figure 1.13, resultant D-A type polymer has a lower band gap with HOMO energy level close to HOMO of the donor moiety and LUMO energy level close to LUMO of the acceptor moiety.

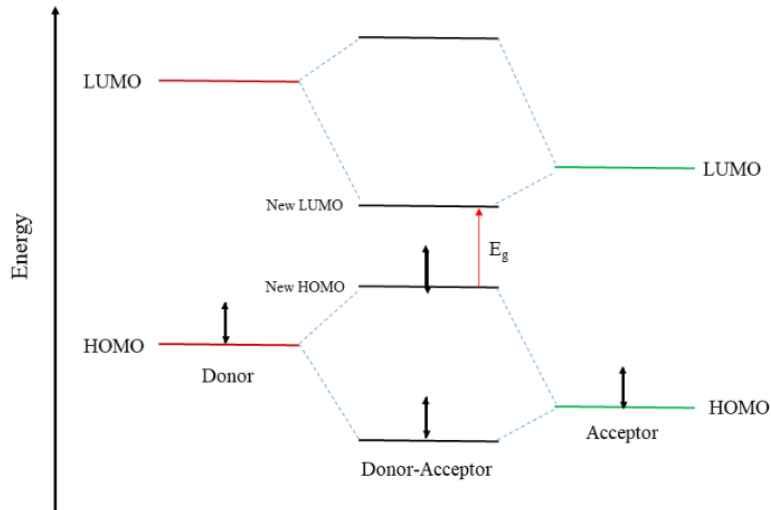


Figure 1.14: Molecular orbital hybridization of energy levels

1.2.3.3.4 Hole Transport Layer (HTL)

For a better device operation in inverted cell, a hole transport layer must be inserted between the organic active layer and top metal anode in order to provide better hole extraction, transportation and collection as well as electron blocking by arranging the proper energy alignment [36]. In inverted organic solar cells, PEDOT:PSS and transition metal oxides (TMOs) like MoO_3 , WO_3 , V_2O_5 are most commonly used HTL layers. However, due to some disadvantages of PEDOT:PSS given in the section 1.2.3 in the device construction, TMOs are generally preferred.

1.2.3.3.4.1 MoO_3

Among all the transition metal oxides, molybdenum oxide (MoO_3) shows a better device performance due to good hole mobility, high work function, easy processing like solution deposition and thermal evaporation deposition and high transmittance. In thermal deposition technique, film thickness in nanometer scale can be controlled by giving dense and uniform MoO_3 film. MoO_3 also prevents fast device degradation by

acting as a barrier to diffusion of oxygen and metal ions inside the active layer.

In 2008, Chen et al demonstrated that device performance of inverted organic solar cell based on P3HT:PCBM active layer increased by deposition of MoO₃ thin film as a HTL. They reported that optimum HTL thickness depends on the top metal electrode. Metals such as Ag, Au and Al have been used to investigate the variation in MoO₃ film thicknesses. Unlike Ag and Au, devices with Al as a top electrode required thicker hole transport layer due to reduction of MoO₃ to MoO₂ during the evaporation process [37]. The effect of MoO₃ thickness on overall device efficiency has been also examined by Zheng and coworkers. They observed decrease in MoO₃ thickness (≤ 5 nm) caused a drop in open circuit voltage (V_{oc}) and fill factor (FF). This behavior was correlated with increase of the series and decrease of the shunt resistance [38].

1.2.3.3.5 Anode

For IOSCs, top metal electrode serves as an anode. The anode should possess high conductivity, high thermal and chemical stability, good film forming ability to have a proper contact with adjacent organic layers. Ag, Au are most commonly used metals for this purpose due to their air-stable natures [39].

1.3 Organic Photovoltaic Parameters

Solar cell behavior under the AM 1.5G illumination is illustrated in Figure 1.14. Depicted parameters such as short circuit current density, open circuit voltage, fill factor and power conversion efficiency are fundamental for explanation of device performance.

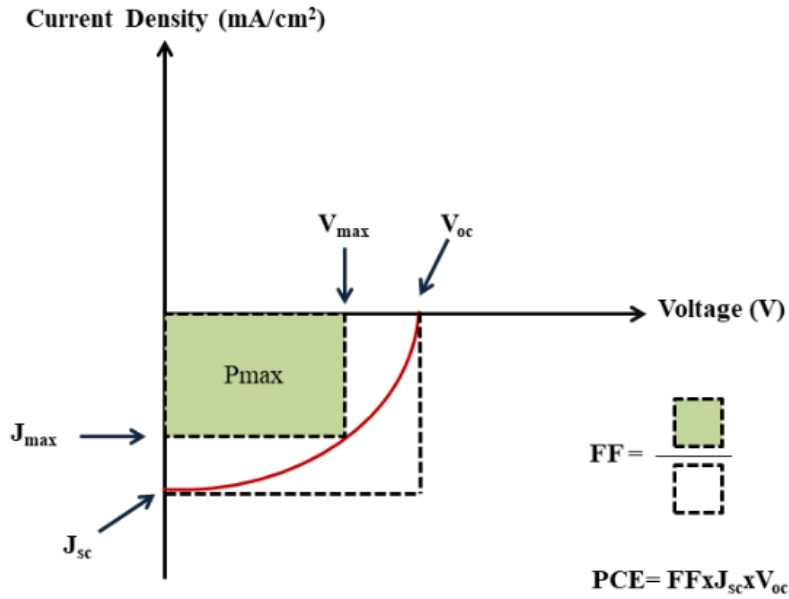


Figure 1.15: The J-V curve of solar cell under illumination

Solar spectrum varies during the day with location. In order to compare the performance of OPVs in the research laboratories, standard reference spectra are defined such as AM 0 G with integrated power of 1366.1 W/m² is used for the space applications, AM 1.5 G with integrated power of 1000 W/m² is for the flat plate modules.

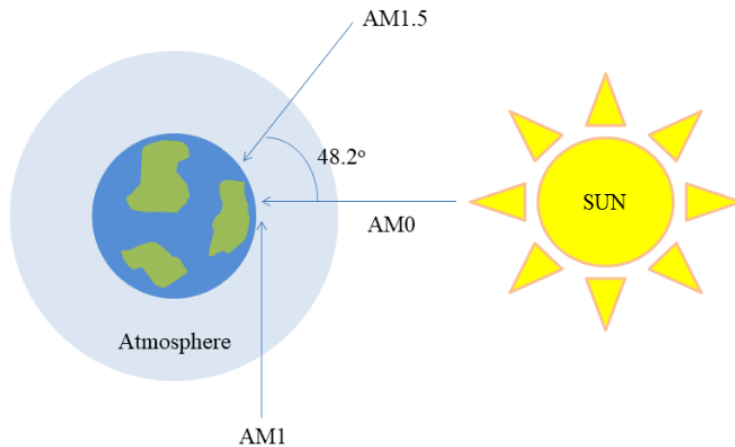


Figure 1.16: AM 1.5G standardization

1.3.1 Short Circuit Current Density (J_{sc})

Short circuit current density is the maximum current when there is no voltage across the solar cell. It gives the amount of charge carriers collected at electrodes. J_{sc} is directly related with light absorption in the device. Therefore, polymers with small band gap harvest more sunlight thus give higher short circuit current values [40].

1.3.2 Open Circuit Voltage (V_{oc})

Open circuit voltage is the maximum voltage when there is no current flow through the circuit. It is correlated with difference between the HOMO of the donor and LUMO of the acceptor. Therefore, during the low band gap polymer design, optimum V_{oc} value should also be considered for higher device efficiency [41].

1.3.3 Fill Factor (FF)

Fill factor is the ratio of the maximum power ($J_{max} \times V_{max}$) to product of J_{sc} and V_{oc} . In a graphical expression, it is a measure of squareness of the solar cell. For an ideal case, FF is equal to unity. However, achieving the high fill factor values in OPVs is not easy to obtain due to several factors such as morphological problems in the cell, improper thickness of the active layer, shunt and series resistance. Morphology of the solar cells requires many optimization studies to attain proper D-A phase separation, domain size, crystallinity etc for obtaining efficient charge mobility [42]. Thickness of the active layer is important for the light absorption but studies have shown that although thicker organic layers absorb higher percentage of the incident light, efficiency of the

device is not high enough due to charge recombination through the longer diffusion length. Shunt resistance arises from current leakage through the cell. If the current finds an alternative pathway to flow in the circuit, it decreases the total charge carrier collection at the anode and cathode electrodes thus lowering the device efficiency. Thus, higher shunt resistance is required for the leakage-free device performance with elevated FF value. Series resistance on the other hand is attributed to the ohmic loss in the cell including the active layer-contact interfaces. Therefore, low series resistance is necessary in order to reduce bulk and contact resistance [43][44].

$$FF = \frac{V_{max} \times J_{max}}{V_{oc} \times J_{sc}} \quad (1)$$

1.3.4 Power Conversion Efficiency (PCE)

PCE is the ratio of maximum generated power to incident power. Irradiance of the incident light by AM 1.5G illumination is 100 W/cm².

$$PCE = FF \times V_{oc} \times J_{sc} \quad (2)$$

1.3.5 External Quantum Efficiency (EQE)

EQE is the ratio of the total extracted charge carriers to incident light. By IPCE (incident photon to current efficiency) measurement, external quantum efficiency of the solar cell is determined.

1.4 Morphology Control in the BHJ Active Layer

Morphology optimization of the active layer in solar cells is one of the most effective strategies to obtain high power conversion efficiency. Therefore, extensive research efforts have been devoted to investigate methodologies for morphology control such as D-A blend ratio, solvent effect, thermal annealing, solvent annealing and introduction of a processing additive.

1.4.1 D-A Blend Ratio

It has been proven that BHJ-type solar cells prepared from blends of electron acceptor and electron donor materials result in better device performance due to the ultrafast electron transfer from donor to acceptor molecules through the large interfacial D-A areas. Therefore, blend ratio of these components must be arranged properly for an efficient charge transportation. Upon from photoexcitation, generated excitons are diffused through the donor and dissociate at the D-A interface. After that, electrons and holes are transported to the corresponding electrodes via percolated acceptor and donor materials. In a perfectly regulated donor-acceptor blend, ratio between the hole and electron mobilities is decreased resulting in a more balanced charge transport. Thus, it is possible to control the morphology of the active layer by providing the optimum donor-acceptor blend which leads to enhanced exciton dissociation and charge transportation throughout the interpenetrated nanoscale network [45][46].

1.4.2 Solvent Effect

Choice of a host solvent significantly influences the morphology of the active layer and thus device performance. Generally, solar cells of high boiling point solvents such as chlorobenzene (CB) and 1,2-dichlorobenzene (DCB) shows better device

performance than low boiling point solvents like chloroform (CF) due to efficient solubility of polymer in the chosen solvent.

Host solvent determines degree of crystallinity, domain size and vertical material distribution. Therefore, the most suitable solvent should be selected for the interested active layer to obtain higher efficiency. Figure 1.16 represents the TEM images of D-A thin films prepared by different solvents. Small and not linked domains cause higher charge recombination. On the other hand, large domains result in less interface areas within the BHJ which reduce exciton separation. Thus, optimum domain size should be achieved. DCB-processed system leads to smaller and penetrated domains in the blend layer. Moreover, mixed solvent method is also useful for some polymer systems. Specifically, some devices made from a CF:DCB solvent system show much better performance than devices fabricated from CF and DCB alone. Mixing high boiling point DCB with volatile CF provides slow evaporation of host solvent which gives the polymer enough time to crystallize [47].

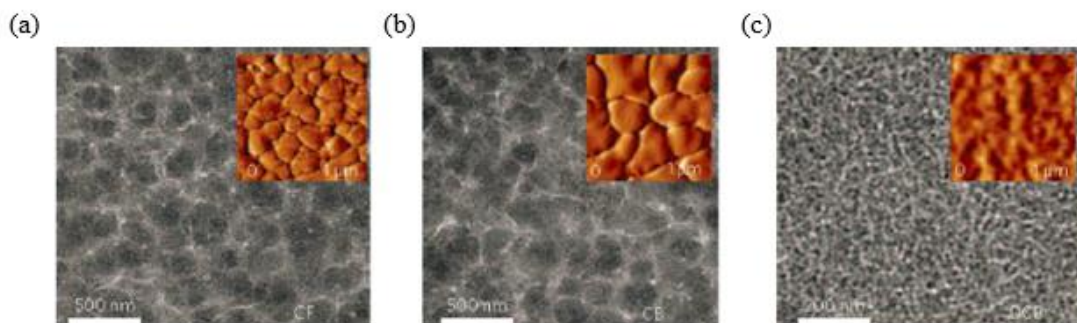


Figure 1.17: TEM images of thin films spin cast from (a) CF, (b) CB, and (c) DCB

1.4.3 Thermal Annealing

Phase separation in the active layer usually begins in the solution but interrupted by the film formation during the spin coating process. Therefore, further modifications

are needed for the improvement of donor-acceptor blend morphology. Recent studies in OPVs have revealed that morphology of the certain type of active layer materials can be controlled by thermal annealing. Improvement in the device performance is attributed to the enhanced crystallinity of polymer resulting in a better charge transport property in the blend. Upon thermal annealing, self-organized active layer leads to red shift in the absorption spectrum due to enhanced interchain interaction of highly ordered, crystalline structure. Transmission electron microscopy (TEM) of the thermally annealed polymer:PCBM films are shown well-developed interpenetrating networks with distinguishable donor-acceptor domains which explains higher PCE [48].

1.4.4 Solvent Annealing

Solvent annealing is an another useful technique to promote the phase separation of BHJ materials. It is a slow growth process which manipulates the orientation of copolymer. Ordering of the copolymer could be initiated at the film surface by controlling the rate of solvent annealing. Solvent imparts mobility of the copolymer, providing the rapid removal of defects. As a result, highly oriented, almost defect-free domains are attained. Atomic force microscopy and grazing incident X-ray diffraction results can provide sufficient evidence with improved morphology of interpenetrating BHJ solar cells by solvent annealing approach[49][50].

1.4.5 Processing Additive

Processing additive offers the simplest and effective way to control the morphology of the active layer compared to the other methods. Introduction of a small amount of additive into donor-acceptor blend is enough for observing the performance improvement. Processing additives have three main properties that are;

- miscible with the host solvent
- less volatile (higher boiling point) than the host solvent
- selective solubility towards to donor or acceptor (generally acceptor such as PCBM)

Domain size of the active layer in a single host solvent is generally too large or too small which is insufficient for the efficient exciton dissociation and charge transportation. However, selectively dissolved PCBM aggregates by additive molecules penetrates into the polymer (donor) chains forming a well phase-separated morphology by eliminating the large domains of pure acceptor material. 1,8-diiodooctane (DIO), 1-chloronaphthalene (CN), diphenylether (DPE) are representative processing additives which enhance the power conversion efficiency by improving the exciton dissociation and charge transportation as well as reducing the charge recombination due to the formation of bicontinuous interpenetrating network between the donor and acceptor materials. Recent studies have proved that unlike other additives, CN and DPE are capable of dissolving both donor and acceptor by pretending like co-solvents. Therefore, higher PCE results are expected to obtain for devices prepared with these additives [51][52].

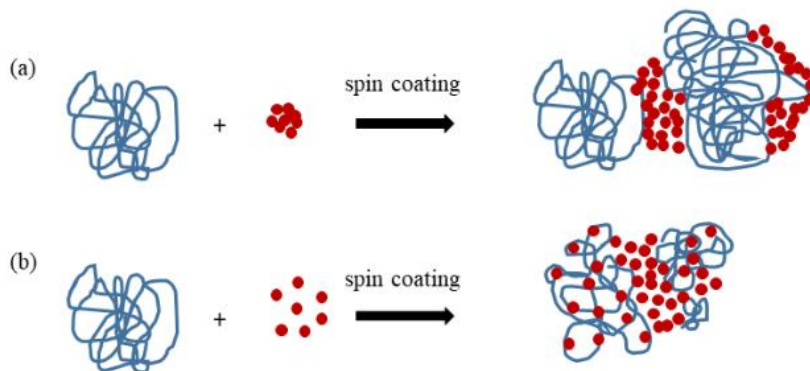


Figure 1.18: Scheme of D-A blend aggregation (a) without additive, (b) with additive

1.5 Aim of the Study

In this thesis study, high performance inverted organic solar cells are aimed to construct. In order to fulfill this aim, donor-acceptor type conjugated polymers with lower band gaps were used as the active layer materials. Structures of the two novel conducting polymers are shown in Figure 1.17. Benzodithiophene which has a strong electron donating ability and planar structure was used as a donor moiety. On the other hand, benzotriazole was used as an acceptor moiety because of its electron deficient nature. Thiophene and selenophene units were incorporated into the polymer backbones as π -bridges in order to enhance the conjugation length. Electrochemical and photovoltaic studies of the polymers P1 and P2 were performed.

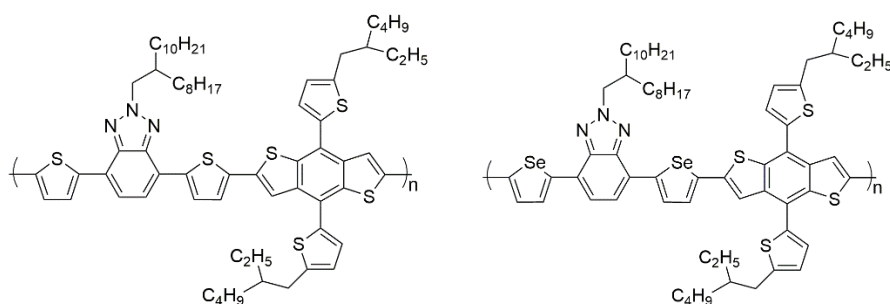


Figure 1.19: Chemical structures of P1 and P2, respectively

CHAPTER 2

EXPERIMENTAL

2.1 Materials

Conducting polymers P1 and P2 were supplied from Çırpan's Research Group. Weight average molecular weights of the polymers were 37 kDa and 21 kDa, respectively. Zinc acetate dihydrate, 2-methoxyethanol, ethanolamine, methanol, toluene, 2-propanol, chlorobenzene, 1,2-dichlorobenzene, diphenylether, 1-chloronaphthalene and 1,8-diiodooctane were purchased from Sigma Aldrich Chemical Co. Ltd. PC₇₁BM was obtained from Ossilla. ITO-glasses were purchased from VisionTek Systems. MoO₃ and Ag were purchased from Kurt J. Lesker. All device fabrications were performed under nitrogen atmosphere unless otherwise mentioned.

2.2 Equipments

Cyclic voltammetry studies were performed in a solution of 0.1 M tetrabutylammonium hexafluorophosphate (TBAPF₆) in acetonitrile (ACN) solution at 100 mVs⁻¹ scan rate. A Gamry 600 potentiostat with three-electrode system was used for this purpose. UV-Vis spectra of the polymers were examined by Varian Cary 5000 UV-Vis spectrophotometer at the room temperature. Molecular weights and polydispersity indexes of the polymers were determined by Shimadzu gel permeation chromatography (GPC). Cleaning of ITO surfaces was carried out in Bandelin Sonorex Ultrasonic Bath. Harrick Plasma Cleaning was used for the further surface cleaning. Organic active layers were spin coated via Sawatec Spinner in the MBraun glovebox system. Evaporation of MoO₃ and Ag were performed in the glovebox by

Nanovak evaporator. The current density-voltage (J-V) measurements of the constructed devices were carried out in the glovebox system ($O_2 < 0.1$ ppm, $H_2O < 0.1$ ppm). J-V characteristics were recorded using a Keitley 2400 Source. Atomic force microscopy (AFM) and transmission electron microscopy (TEM) were used for surface and morphology imaging at METU Central Laboratory.

2.3 Synthesis of Polymers

Polymer P1 and P2 were synthesized via Stille crosscoupling polymerization in the presence of bis(triphenylphosphine)palladium(II)dichloride catalyst under inert atmosphere. The number average molecular weight and the weight average molecular weight of P1 were determined as 15 kDa and 37 kDa, respectively. The polydispersity index of P1 is 2.47. For P2, the number average molecular weight and the weight average molecular weight were obtained as 7 kDa and 21 kDa. The polydispersity index of it is 3.

2.4 Electrochemical Studies

For cyclic voltammetry studies of P1 and P2, polymers were dissolved in chloroform (5 mg/ml) and spray coated onto ITO-glass substrate using Omni spray coating gun. A set-up containing three-electrode system was constructed. ITO substrate was used as a working electrode. A Pt wire was operated as a counter electrode and a Ag wire which was calibrated against Fc/Fc⁺ reference electrode was used as the reference electrode. Polymer coated ITO-glasses were dipped into 0.1 M TBAPF₆ supporting electrolyte in order to conduct electrochemical studies.

By means of cyclic voltammetry studies, redox properties of the polymers were investigated. Reversible responses towards positive and negative potentials concluded ambipolar (both p and n dopable) characters of the polymers. HOMO and LUMO

energy levels were detected from the onset of the oxidation of p-doping states and reduction of n-doping states, respectively. From the calculated HOMO and LUMO energy levels, electronic band gaps of the polymers were obtained.

2.5 Optical Studies

Absorption spectra of the polymers in both solution and as a thin film were run in order to detect absorption ranges, maximum absorption and onset wavelengths as well as calculating optical band gaps of the polymers.

2.6 Photovoltaic Studies

Inverted organic photovoltaic applications of polymers were constructed as following ITO / ZnO / POLYMER:PC₇₁BM / MoO₃ / Ag. Diphenyl ether, 1-chloronaphthalene and 1,8-diiodooctane additives were used in order to enhance the power conversion efficiencies of the solar cells.

2.6.1 Device Fabrication of IOSCs

2.6.1.1 ITO Cleaning

ITO coated glass sheets were etched with hydrochloric and nitric acid solutions (96:4) to avoid short-circuit as well as to reduce the device area. Cleaning step must be performed gently and properly in order to prevent any defects in organic layers. Therefore, ITO substrates were sonicated in toluene, detergent water (Hellmanex III), distilled water and 2-propanol for 15 minutes. After that, substrates were dried under nitrogen gas and subjected to oxygen plasma for 5 minutes to remove organic

impurities on the ITO surfaces. Also, work function of ITO surface increases by plasma cleaning which creates a more hydrophilic surface.

2.6.1.2 Electron Transport Layer (ZnO)

Zinc oxide solution prepared using zinc acetate dihydrate, 2-methoxyethanol and ethanolamine was filtered from 0.22 μm PTFE membrane and spin coated on cleaned ITO surface with 4000 rpm to attain a smooth electron transport layer. Coated substrates were annealed at 150 C° for 20 minutes.

2.6.1.3 Active Layer

Polymer and PCBM blends in active layer were prepared with different ratios and concentrations in varied solutions to find the optimum composition. Moreover, DPE, DIO and CN additives were used in several amounts until the best device performance was achieved. Then, active layer solutions were filtered from 0.45 μm PTFE membrane and spin coated with different rpms for optimization of film thicknesses. All of these process were carried out under the nitrogen atmosphere in glovebox.

2.6.1.4 Thermal Evaporation

5 nm MoO_3 and 100 nm Ag were thermally evaporated with an average rate of 1.0 A°/s and 2.5 A°/s, respectively in the glovebox system. A thin layer of MoO_3 serves as a hole transport layer which provides energy alignment between the layers and acts like a buffer layer for protecting active layer during the thermal deposition of Ag.

2.6.2 Characterization of IOSCs

J-V curves of the fabricated solar cells were recorded with a Keitley 2400 source meter under AM 1.5G solar illumination (100 mWcm^{-2}). Incident photon to current efficiencies (IPCE) of the solar cells were determined by the Oriel quantum efficiency measurement system from 300 nm to 900 nm.

CHAPTER 3

RESULTS AND DISCUSSION

3.1 Electrochemical Studies

Electrochemical studies were carried out in order to determine HOMO-LUMO energy levels and electronic band gaps of the polymers. For cyclic voltammetry, polymers dissolved in chloroform (5 mg/ml) and spray coated onto ITO substrates. ITO glass, Pt and Ag wire were placed in a quartz cell. TBAPF₆ in acetonitrile was used as the supporting electrolyte. All cyclic voltammetry measurements were carried out at 100 mVs⁻¹ scan rate.

Cyclic voltammograms of the polymers are illustrated in Figure 3.1. Both polymers are p and n dopable hence, HOMO and LUMO energy levels were calculated from the onset of the oxidations of p-doping states and reductions of the n-doping states, respectively. Reversible redox couple of P1 in the p-type doping/dedoping processes was seen at 0.95 V and 0.74 V, redox couple for P2 was at 0.80 V, 0.59 V. The respective n-type doping/dedoping redox couples were located at -1.89 V and -1.57 V for P1 and at -1.71 V and -1.35 V for P2. The onset of the oxidations at the p-doping states were 0.55 V and 0.53 V for P1 and P2, respectively. The onset of the reductions at the n-doping states were -1.65 V for P1 and -1.43 V for P2. Using equations 3 and 4, HOMO and LUMO energy levels of the polymers were determined. P1 has a HOMO energy level at -5.30 eV and LUMO energy level at -3.10 eV. On the other hand, P2 possesses a HOMO energy level at -5.28 eV and LUMO energy level at -3.32 eV. From equation 5, electronic band gaps of the P1 and P2 were calculated as 2.20 eV and 1.96 eV, respectively.

$$HOMO = -(E_{ox\ onset} + 4.75)eV \quad (3)$$

$$LUMO = -(E_{red\ onset} + 4.75)eV \quad (4)$$

$$E_g^{el} = (HOMO - LUMO)eV \quad (5)$$

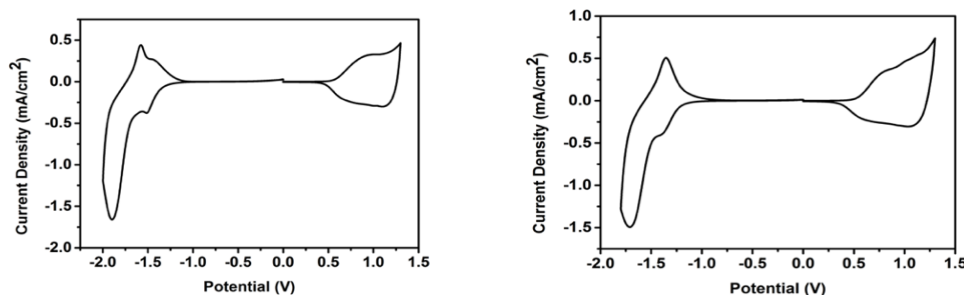


Figure 3.1: Cyclic Voltammograms of the P1 and P2, respectively in 0.1 M TBAPF₆/ACN

Incorporation of the π -bridge into polymer backbone not only provides higher conjugation length and reduced steric hindrance in the polymer chains but also influences electronic and optical properties of the polymer. In this study, thiophene and selenophene units were used as π -bridges. Replacement of sulfur atom for selenium in the polymer backbone showed only a small influence in HOMO energy level due to small electronegativity difference between the sulfur and selenium heteroatoms. Therefore, devices based on P1 and P2 maintain similar V_{oc} values as a result of similar HOMO energy levels. On the other hand, significant change was observed in LUMO energy levels because of the stabilizing effect of heteroatoms which is directly related to the ionization potentials. Since ionization potential of selenium is smaller than sulfur, P2 with selenophene π -bridge leads to a deeper LUMO energy level (-3.32 eV) than P1 thiophene one (-3.10) which results in reduced band gap [53]. Table 3.1 represents all the electrochemical results of the polymers in detail.

Table 3.1 Summary of the electrochemical studies

Polymer	$E_{p-doping}$ (V)	$E_{p-dedoping}$ (V)	$E_{n-doping}$ (V)	$E_{n-dedoping}$ (V)	HOMO (eV)	LUMO (eV)	E_g^{el} (eV)
P1	0.95	0.74	-1.89	-1.57	-5.30	-3.10	2.20
P2	0.80	0.59	-1.71	-1.35	-5.28	-3.32	1.96

3.2 Optical Studies

Absorption range of benzodithiophene and benzotriazole bearing copolymers were determined by UV-Vis spectroscopy as depicted in Figure 3.2. Maximum absorption bands at neutral states were observed at 519 nm and 540 nm which corresponds to $\pi-\pi^*$ transition for P1 and P2, respectively. Optical band gaps of the polymers were obtained from the onset of the neutral state absorption. The onsets are located at 636 nm for P1 and 664 nm for P2. From the equation 6, optical band gaps were calculated as 1.95 eV and 1.87 eV. Red shifts in absorption spectra of the P1 and P2 based thin films were attributed to enhance intermolecular interactions through the polymer chains in the solid state which increased in $\pi-\pi$ stacking and aggregation tendency. Note that electronic band gap of the polymers are higher than the optical band gaps because of applied electron binding energy. Table 3.2 summarizes optical study results of the polymers.

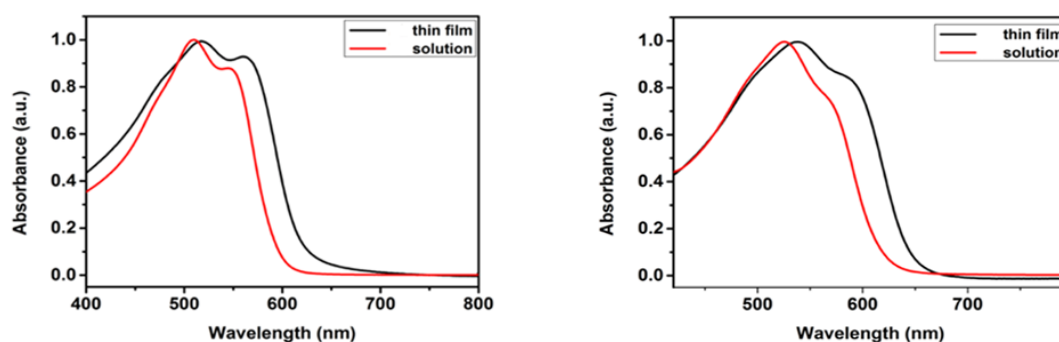


Figure 3.2: Absorption spectra of P1 and P2, respectively

$$E_g^{op} = \frac{1241}{\lambda_{onset}} \quad (6)$$

Table 3.2 Summary of the optical studies

Polymer	λ_{max} (nm)	E_g^{op} (eV)
P1	519/561	1.95
P2	540/590	1.87

3.3 Photovoltaic Studies

Device applications of benzodithiophene and benzotriazole bearing alternating copolymers were performed. In order to examine the π -bridge effect on charge carrier mobility, thiophene (P1) and selenophene (P2) units were incorporated into polymer backbones. For photovoltaic properties of the polymers, inverted organic solar cells were fabricated with a device architecture of ITO/ZnO/Polymer:PC₇₁BM /MoO₃ (5

nm)/Ag (100 nm). Blend ratio and concentrations, active layer thicknesses, different additives with various concentrations were optimized in order to obtain the best device performance. Solvent optimization was also carried out to enhance the polymer solubility as well as improving the exciton dissociation and charge carrier transportation. In this content, polymer and PC₇₁BM blends dissolving in chlorobenzene resulted in the best morphology. Instead of using PC₆₁BM, PC₇₁BM was selected due to its absorption in the visible region which enhances absorption of the blend. Current density / Voltage (J/V) characteristics of the IOSCs were shown in Figure 3.2 for P1 and Figure 3.3 for P2.

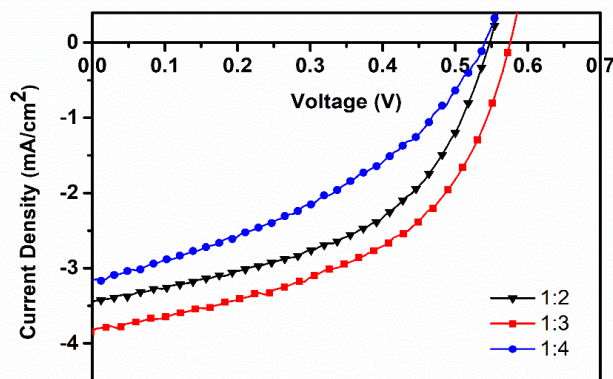


Figure 3.3: J-V curve of IOSCs based on P1:PC₇₁BM blend ratios

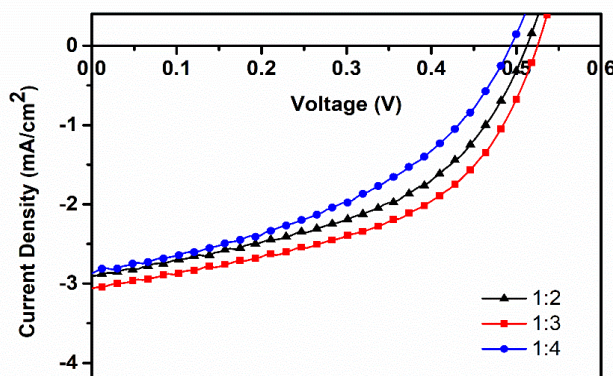


Figure 3.4: J-V curve of IOSCs based on P2:PC₇₁BM blend ratios

1:3 blend ratio showed the best device performance for both P1 and P2 based solar cells. Increasing PC₇₁BM ratio from 1:2 to 1:3 improved the charge transport ability for both polymers which resulted in enhanced PCE. However, further increase in PC₇₁BM ratio decreased contribution of the polymer on absorption thus reduced the short-circuit current density (J_{sc}). Table 3.3 and 3.4 are summarized the photovoltaic properties of P1 and P2, respectively.

Table 3.3: Summary of the photovoltaic studies of P1

Polymer(P1):PC ₇₁ BM (w:w)	J_{sc} (mA/cm ²)	V_{oc} (V)	J_{max} (mA/cm ²)	V_{max} (V)	FF%	Efficiency%	Solvent	RPM	Treatment
1:2 (2%)	3.4471	0.55	2.3889	0.39	49.14	0.94	cb	750	-
1:3 (2%)	3.8067	0.58	2.5439	0.43	49.54	1.09	cb	750	-
1:4 (2%)	3.1629	0.54	2.1214	0.31	38.50	0.65	cb	750	-
1:3 (2%)	3.8753	0.47	2.8750	0.34	53.66	0.97	o-dcb	750	-
1:3 (3%)	3.9458	0.59	2.5945	0.43	47.92	1.13	cb	750	-
1:3 (3.5%)	2.5988	0.61	1.6153	0.45	45.85	0.72	cb	750	-
1:3 (3%)	2.7269	0.60	2.0389	0.43	53.59	0.87	cb	500	-
1:3 (3%)	3.2486	0.55	1.9784	0.33	36.54	0.64	cb	1000	-
1:3 (3%)	3.3902	0.58	2.9038	0.37	54.64	1.06	cb	750	1.5% DIO
1:3 (3%)	3.5239	0.58	2.8899	0.38	53.73	1.10	cb	750	2% DIO
1:3 (3%)	3.1150	0.54	1.8765	0.34	37.92	0.64	cb	750	3% CN
1:3 (3%)	3.6395	0.58	2.9719	0.42	59.13	1.23	cb	750	6% CN
1:3 (3%)	3.4438	0.59	2.3284	0.40	45.84	0.93	cb	750	9% CN
1:3 (3%)	4.5103	0.52	3.4842	0.37	54.97	1.30	cb	750	3% DPE
1:3 (3%)	-	-	-	-	-	-	cb	750	3% DPE + MeOH

Table 3.4: Summary of the photovoltaic studies of P2

Polymer(P2):PC ₇₁ BM (w:w)	J_{sc} (mA/cm ²)	V_{oc} (V)	J_{max} (mA/cm ²)	V_{max} (V)	FF%	Efficiency%	Solvent	RPM	Treatment
1:2 (2%)	2.9066	0.52	1.9456	0.36	46.34	0.70	cb	750	-
1:3 (2%)	3.0633	0.53	1.9741	0.39	47.42	0.77	cb	750	-
1:4 (2%)	2.8678	0.52	1.9561	0.39	51.16	0.75	cb	750	-
1:3 (3%)	3.3937	0.52	2.2573	0.35	44.77	0.79	cb	750	-
1:3 (3.5%)	2.8711	0.51	1.9695	0.34	45.73	0.68	cb	750	-
1:3 (3%)	3.3013	0.52	2.2504	0.37	48.50	0.83	cb	500	-
1:3 (3%)	3.6679	0.51	2.6125	0.36	50.28	0.94	cb	1000	-
1:3 (3%)	3.1748	0.51	2.0292	0.33	41.36	0.67	cb	1000	3% DPE
1:3 (3%)	3.2445	0.53	2.0328	0.39	46.10	0.78	cb	1000	1.5% CN
1:3 (3%)	3.7920	0.52	3.0166	0.34	52.01	1.02	cb	1000	3% CN
1:3 (3%)	3.4076	0.52	2.1646	0.37	45.20	0.80	cb	1000	4% CN
1:3 (3%)	3.8336	0.49	2.6281	0.34	47.57	0.90	cb	1000	3% CN, MeOH

Then, active layer thicknesses were optimized in order to balance the light absorption and charge transport. Although thicker films are more favorable due to better absorption of the incident light, there is a huge possibility of recombination of charge carriers through the longer travel distance. Moreover, thicker films possess lower shunt resistance and higher series resistance which decreases the device performance substantially. Therefore, optimum film thickness must be achieved for a high PCE. The optimum film thickness was found as 120 nm for P1 in 750 rpm and 90 nm for P2 in 1000 rpm. Thickness investigations of the polymers were done by Atomic Force Microscopy (AFM).

CN, DIO and DPE were used as processing additives to enhance J_{sc} and FF of the solar cells. The effects of these additives on J-V curves of the polymers were illustrated in Figure 3.4 and 3.5.

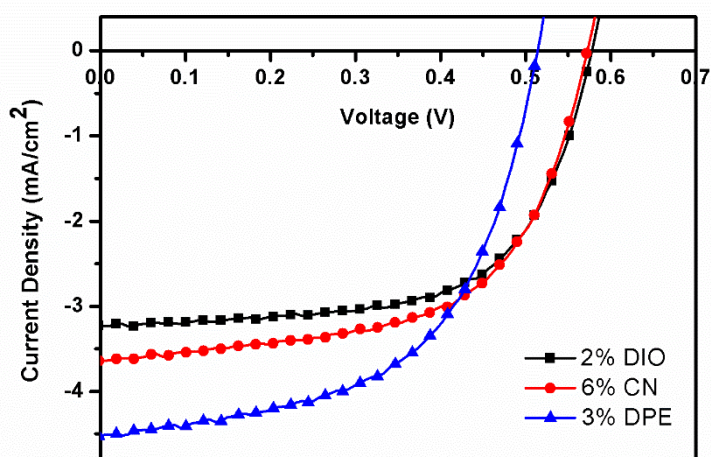


Figure 3.5: J-V curves of P1 in different additives

Several experiments were conducted to determine the most suitable additive with proper concentration. As a result, P1:PC₇₁BM active layer with 1:3 blend ratio containing 3% DPE showed the highest PCE of 1.30% with J_{sc} of 4.51 mA/cm², V_{oc} of 0.52 V and FF of 54.97%.

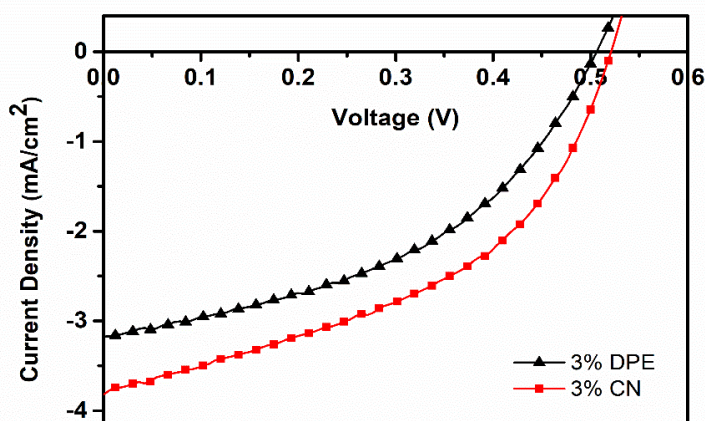


Figure 3.6: J-V curves of P2 in different additives

Blend ratio, solution concentration, film thickness were determined for P2 as well. DIO based solar cells showed extremely poor blend morphology thus, DPE and CN additions were examined exclusively. Thus, P2:PC₇₁BM active layer with 1:3 blend ratio containing 3% CN resulted in the highest PCE of 1.02% with J_{sc} of 3.79 mA/cm², V_{oc} of 0.52 V and FF of 52.01%.

In order to investigate the effect of additives in polymer morphologies, transmission electron microscopy (TEM) images were examined. Figure 3.7 represents the TEM images of polymers. As seen, both P1 and P2 based active layers without additive have larger and discrete domains which inhibits the efficient exciton dissociation at the D-A interface and charge transportation. On the other hand, TEM images of additive based polymer blends result in smaller domains with interpenetrated bicontinuous networks that provides effective exciton dissociation as well as improved charge transportation and collection. As a result, PCE of P1 based device was improved from 1.13% to 1.30% via 3% DPE while P2 based solar cell was improved from 0.94% to 1.02% via 3% CN due to enhanced J_{sc} and FF values. Note that CN and DPE based solar cells showed better performance than DIO based ones because the former additives dissolve both polymer and PC₇₁BM materials which act like co-solvents.

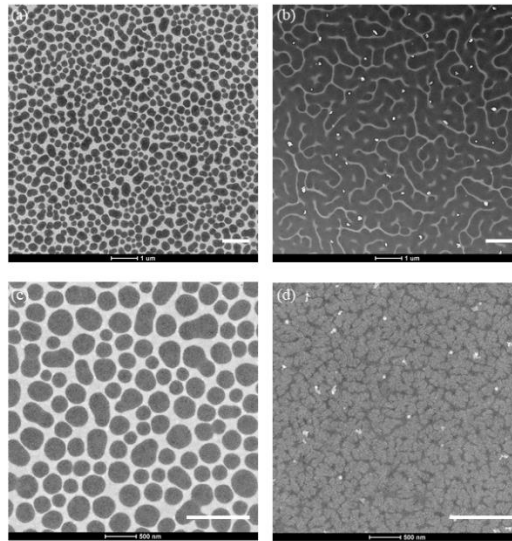


Figure 3.7: TEM images of (a) P1:PC₇₁BM (1 μm), (b) P1:PC₇₁BM+3% DPE (1 μm), (c) P2:PC₇₁BM (500 nm), (d) P2: PC₇₁BM +3% CN (500 nm)

Methanol treatment was also performed after spin coating of the active layers. The aim of this method was optimization of the phase separation and eliminating the traps on the surface of the solar cell devices as well as removal of excess additive residuals. However, no improvement in PCEs was observed for both P1 and P2 based devices [54].

Incident photon to current efficiency measurement were performed after all optimization experiments were carried out. External quantum efficiencies of P1 and P2 based solar cells with the best results were determined as 32% and 23%.

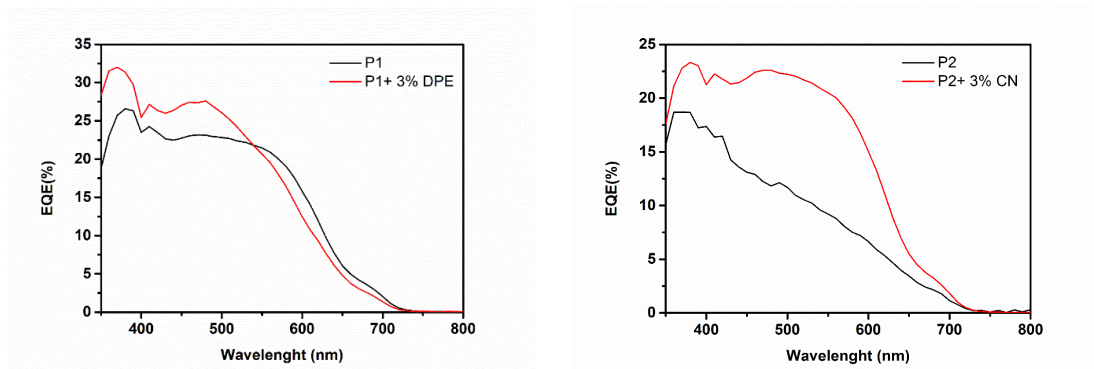


Figure 3.8: IPCE curves of the best performance solar cells of P1 and P2

Power conversion efficiency of the thiophene π -bridge incorporated polymer P1 exhibited higher than that of the selenophene π -bridge incorporated polymer P2 although opposite of this situation was expected due to the lower band gap of the P2. Therefore, possible reasons can be listed for explanation. Firstly, molecular weight plays an important role in the blend morphology. Increasing molecular weight enhances light absorption, short circuit current density and hole mobility. It also increases the fill factor of the devices due to better thin film forming ability. Thus, lower molecular weight of P2 (21 kDa) than P1 (37 kDa) could have an influence on this situation. Secondly, selenophene based polymers generally necessitate slightly thinner active layers which leads to less efficient light harvesting and poor hole mobility thus decreases the J_{sc} and naturally PCE of the devices. In this study, selenophene based P2 was spin coated at relatively higher rpm (1000) compare to thiophene based P1 (750) that clarifies the lower J_{sc} and PCE values of P2. Thirdly, molar absorption coefficients (determined in solution) of the selenophene based polymers are in most cases lower than thiophene based polymers which limits the light absorption of these devices by causing poor J_{sc} and PCE [55]. Experimental results showed in Appendix B revealed that molar absorption coefficient of the P2 ($855 \times 10^6 \text{ Lmol}^{-1}\text{cm}^{-1}$) is lower than molar absorption coefficient of the P1 ($952 \times 10^6 \text{ Lmol}^{-1}\text{cm}^{-1}$) which explains the reduced PCE for P2. In addition to that reasons, high number of pinholes in the active layers of P1 and especially P2 imaged via transmission electron microscopy can explain why selenophene based polymer resulted in a lower PCE than thiophene based one as well as explaining the overall low results for these polymers. Presence of pinholes damages the active layer morphology by affecting series resistance and reducing shunt resistance which causes higher leakage current [47].

CHAPTER 4

CONCLUSION

Electrochemical, optical and photovoltaic studies of the two novel benzodithiophene and benzotriazole bearing alternating copolymers were carried out. Cyclic voltammetry was performed in order to determine HOMO-LUMO energy levels and electronic band gaps of the polymers. According to the cyclic voltammograms, HOMO and LUMO energy levels of the P1 and P2 were calculated as -5.30 eV / -3.10 eV and -5.27 eV / -3.32 eV, respectively. From the calculated energy levels, electronic band gaps of the polymers were determined as 2.20 eV for P1 and 1.96 eV for P2. Optical band gaps of the P1 and P2 were found from the onset of the π - π^* transition of the neutral film as 1.95 eV and 1.87 eV, respectively.

Inverted organic photovoltaic applications of polymers were constructed as following ITO / ZnO / POLYMER:PC₇₁BM / MoO₃ / Ag. Several optimization studies were carried out in order to find the best device performance. As a result of them, P1 with 1:3 blend ratio in chlorobenzene solvent in the presence of 3% DPE showed 1.30% of PCE with 4.5103 mA/cm² J_{sc}, 0.52 V V_{oc}, 54.97 % FF. For P2, 1:3 blend ratio in chlorobenzene solvent in the presence of 3% CN gave 1.02% of PCE with 3.7920 mA/cm² J_{sc}, 0.52 V V_{oc}, 52.01 % FF. The active layer morphologies were analyzed by AFM and TEM techniques. Finally, external quantum efficiencies of the P1 and P2 were determined as 34% and 23%, respectively via IPCE measurements.

REFERENCES

- [1] Y. Cal, "Superconductivity in Polysulfur nitride (SN)_x," vol. 34, no. 10, pp. 8–10, 1975.
- [2] C. M. Mikulski, P. J. Russo, M. S. Saran, A. G. MacDiarmid, A. F. Garito, and A. J. Heeger, "Synthesis and Structure of Metallic Polymeric Sulfur Nitride, (SN)_x, and Its Precursor, Disulfur Dinitride, S₂N₂," *J. Am. Chem. Soc.*, vol. 97, no. 22, pp. 6358–6363, 1975.
- [3] W. J. Feast, J. Tsibouklis, K. L. Pouwer, L. Groenendaal, and E. W. Meijer, "Synthesis, processing and material properties of conjugated polymers," *Polymer (Guildf.)*, vol. 37, no. 22, pp. 5017–5047, 1996.
- [4] E. S. R *et al.*, "Electronic properties of non-doped and doped polyacetylene films," 1979.
- [5] C. J. Brabec, N. S. Sariciftci, and J. C. Hummelen, "Plastic solar cells," *Adv. Funtional Mater.*, vol. 11, no. 1, pp. 15–26, 2001.
- [6] S. Günes, H. Neugebauer, and N. S. Sariciftci, "Conjugated polymer-based organic solar cells," *Chem. Rev.*, vol. 107, no. 4, pp. 1324–1338, 2007.
- [7] T. K. Das and S. Prusty, "Review on Conducting Polymers and Their Applications," *Polym. Plast. Technol. Eng.*, vol. 51, no. 14, pp. 1487–1500, 2012.
- [8] R. J. Mortimer, D. R. Rosseinsky, and P. M. S. Monk, "Electrochromic Materials and Devices," *Electrochromic Mater. Devices*, vol. 77, pp. 1–638, 2015.
- [9] T.-H. Le, Y. Kim, and H. Yoon, "Electrical and Electrochemical Properties of Conducting Polymers," *Polymers (Basel)*, vol. 9, no. 4, p. 150, 2017.
- [10] J. L. Bredas and G. B. Street, "Polarons, Bipolarons, and Solitons in Conducting Polymers," *Acc. Chem. Res.*, vol. 18, no. 10, pp. 309–315, 1985.

- [11] L. Wu *et al.*, “Effects of the electrode modification conditions on the performance of three-state electrochromic devices via spin-coating,” *Int. J. Electrochem. Sci.*, vol. 12, no. 8, pp. 7712–7727, 2017.
- [12] H. Kallmann and M. Pope, “Photovoltaic effect in organic crystals,” *J. Chem. Phys.*, vol. 30, no. 2, pp. 585–586, 1959.
- [13] C. W. Tang and S. A. Vanslyke, “Organic electroluminescent diodes,” *Appl. Phys. Lett.*, vol. 51, no. 12, pp. 913–915, 1987.
- [14] J. H. Burroughes *et al.*, “Light-emitting diodes based on conjugated polymers,” *Nature*, vol. 347, no. 6293, pp. 539–541, 1990.
- [15] J. R. Lakowicz, *Principles of Fluorescence Spectroscopy Principles of Fluorescence Spectroscopy*. 2006.
- [16] C. W. Tang, “Two-layer organic photovoltaic cell,” *Appl. Phys. Lett.*, vol. 48, no. 2, pp. 183–185, 1986.
- [17] B. Kraabel, C. H. Lee, D. McBranch, D. Moses, N. S. Sariciftci, and A. J. Heeger, “Reprint of: Ultrafast photoinduced electron transfer in conducting polymer-buckminsterfullerene composites,” *Chem. Phys. Lett.*, vol. 589, no. 3, pp. 63–66, 2013.
- [18] G. Zhang *et al.*, “High-Performance Ternary Organic Solar Cell Enabled by a Thick Active Layer Containing a Liquid Crystalline Small Molecule Donor,” *J. Am. Chem. Soc.*, vol. 139, no. 6, pp. 2387–2395, 2017.
- [19] S. Li *et al.*, “Energy-Level Modulation of Small-Molecule Electron Acceptors to Achieve over 12% Efficiency in Polymer Solar Cells,” *Adv. Mater.*, vol. 28, no. 42, pp. 9423–9429, 2016.
- [20] W. Zhao *et al.*, “Molecular Optimization Enables over 13% Efficiency in Organic Solar Cells,” *J. Am. Chem. Soc.*, vol. 139, no. 21, pp. 7148–7151, 2017.
- [21] P. Tehrani, A. Kancierzewska, X. Crispin, N. D. Robinson, M. Fahlman, and M. Berggren, “The effect of pH on the electrochemical over-oxidation in PEDOT:PSS films,” *Solid State Ionics*, vol. 177, no. 39–40, pp. 3521–3527,

2007.

- [22] M. Kemerink, S. Timpanaro, M. M. De Kok, E. A. Meulenkaamp, and F. J. Touwslager, “Three-dimensional inhomogeneities in PEDOT:PSS films,” *J. Phys. Chem. B*, vol. 108, no. 49, pp. 18820–18825, 2004.
- [23] K. Norrman, M. V. Madsen, S. A. Gevorgyan, and F. C. Krebs, “Degradation patterns in water and oxygen of an inverted polymer solar cell,” *J. Am. Chem. Soc.*, vol. 132, no. 47, pp. 16883–16892, 2010.
- [24] X. Yang *et al.*, “Nanoscale morphology of high-performance polymer solar cells,” *Nano Lett.*, vol. 5, no. 4, pp. 579–583, 2005.
- [25] F. Zhang, D. Wu, Y. Xu, and X. Feng, “Thiophene-based conjugated oligomers for organic solar cells,” *J. Mater. Chem.*, vol. 21, no. 44, p. 17590, 2011.
- [26] G. Yu, J. Gao, J. C. Hummelen, F. Wudl, and A. J. Heeger, “Polymer Photovoltaic Cells: Enhanced Efficiencies via a Network of Internal Donor-Acceptor Heterojunctions,” *Science (80-.)*, vol. 270, no. 5243, pp. 1789–1791, 1995.
- [27] M. C. Scharber and N. S. Sariciftci, “Efficiency of bulk-heterojunction organic solar cells,” *Prog. Polym. Sci.*, vol. 38, no. 12, pp. 1929–1940, 2013.
- [28] K. Wang, C. Liu, T. Meng, C. Yi, and X. Gong, “Inverted organic photovoltaic cells,” *Chem. Soc. Rev.*, vol. 45, no. 10, pp. 2937–2975, 2016.
- [29] R. Schlaf, H. Murata, and Z. . Kafafi, “Work function measurements on indium tin oxide films,” *J. Electron Spectros. Relat. Phenomena*, vol. 120, no. 1–3, pp. 149–154, 2001.
- [30] M. S. White, D. C. Olson, S. E. Shaheen, N. Kopidakis, and D. S. Ginley, “Inverted bulk-heterojunction organic photovoltaic device using a solution-derived ZnO underlayer,” *Appl. Phys. Lett.*, vol. 89, no. 14, pp. 87–90, 2006.
- [31] S. Lattante, “Electron and Hole Transport Layers: Their Use in Inverted Bulk Heterojunction Polymer Solar Cells,” *Electronics*, vol. 3, no. 1, pp. 132–164, 2014.

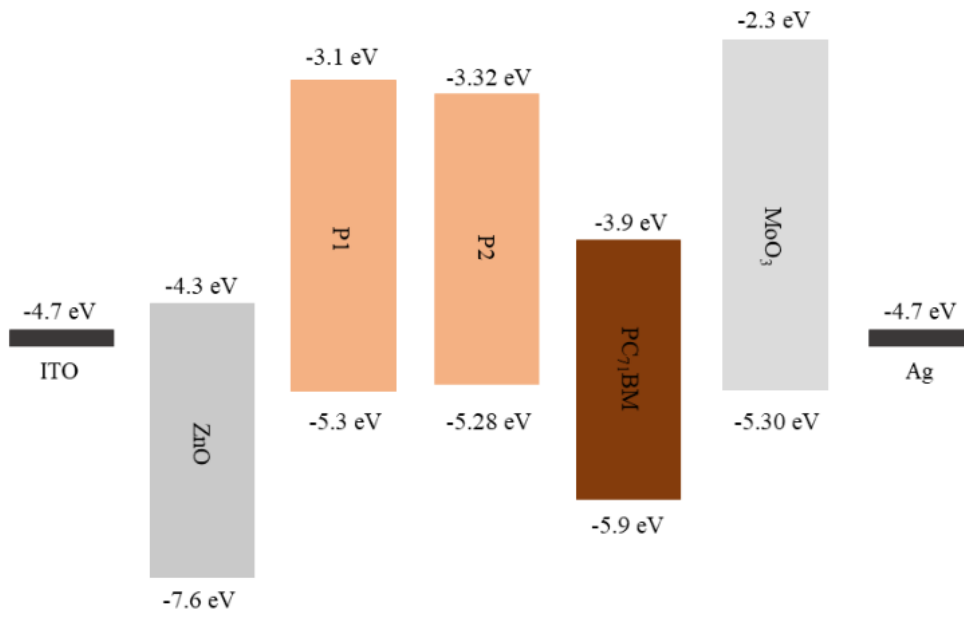
- [32] Z. Hu, J. Zhang, and Y. Zhu, "Inverted polymer solar cells with a boron-doped zinc oxide layer deposited by metal organic chemical vapor deposition," *Sol. Energy Mater. Sol. Cells*, vol. 117, pp. 610–616, 2013.
- [33] C.-Z. Li, H.-L. Yip, and A. K.-Y. Jen, "Functional fullerenes for organic photovoltaics," *J. Mater. Chem.*, vol. 22, no. 10, p. 4161, 2012.
- [34] C. B. Nielsen, S. Holliday, H.-Y. Chen, S. J. Cryer, and I. McCulloch, "Non-Fullerene Electron Acceptors for Use in Organic Solar Cells," *Acc. Chem. Res.*, vol. 48, no. 11, pp. 2803–2812, 2015.
- [35] B. G. Kim *et al.*, "Energy level modulation of HOMO, LUMO, and band-gap in conjugated polymers for organic photovoltaic applications," *Adv. Funct. Mater.*, vol. 23, no. 4, pp. 439–445, 2013.
- [36] J. D. Servaites, M. A. Ratner, and T. J. Marks, "Organic solar cells: A new look at traditional models," *Energy Environ. Sci.*, vol. 4, no. 11, p. 4410, 2011.
- [37] C. Tao *et al.*, "Performance improvement of inverted polymer solar cells with different top electrodes by introducing a MoO₃ buffer layer," *Appl. Phys. Lett.*, vol. 93, no. 19, p. 193307, 2008.
- [38] H. Kim, A. R. bin M. Yusoff, H. Kim, H. Lee, G. Seo, and J. Jang, "Inverted organic photovoltaic device with a new electron transport layer," *Nanoscale Res. Lett.*, vol. 9, no. 1, p. 150, 2014.
- [39] M. Stassel, J. Staudigel, F. Steuber, J. Simmerer, and A. Winnacker, "Impact of the cathode metal work function on the performance of vacuum-deposited organic light emitting devices," *Appl. Phys. A - Mater.*, vol. 390, pp. 387–390, 1999.
- [40] H. Dong and W. Hu, "Organic nanomaterials," *Springer Handb. Nanomater.*, pp. 905–939, 2013.
- [41] N. K. Elumalai and A. Uddin, "Open circuit voltage of organic solar cells: an in-depth review," *Energy Environ. Sci.*, vol. 9, no. 2, pp. 391–410, 2016.
- [42] B. Ray, M. A. Alam, B. Ray, S. Member, and M. A. Alam, "Achieving Fill

Factor Above 80 % in Organic Solar Cells by Charged Interface Achieving Fill Factor Above 80 % in Organic Solar Cells by Charged Interface,” 2012.

- [43] M.-H. Jao, H.-C. Liao, and W.-F. Su, “Achieving a high fill factor for organic solar cells,” *J. Mater. Chem. A*, vol. 4, no. 16, pp. 5784–5801, 2016.
- [44] J.-W. Kang *et al.*, “Reduction of Series Resistance in Organic Photovoltaic Using Low Sheet Resistance of ITO Electrode,” *Electrochem. Solid-State Lett.*, vol. 12, no. 3, p. H64, 2009.
- [45] V. D. Mihailetschi *et al.*, “Compositional dependence of the performance of poly(p-phenylene vinylene):Methanofullerene bulk-heterojunction solar cells,” *Adv. Funct. Mater.*, vol. 15, no. 5, pp. 795–801, 2005.
- [46] P. Kovacic, H. E. Assender, and A. A. R. Watt, “Morphology control in co-evaporated bulk heterojunction solar cells,” *Sol. Energy Mater. Sol. Cells*, vol. 117, pp. 22–28, 2013.
- [47] B. Y. Kadem, A. K. Hassan, and W. Cranton, “The effects of organic solvents and their co-solvents on the optical, structural, morphological of P3HT:PCBM organic solar cells,” vol. 020006, no. 2016, p. 020006, 2016.
- [48] B. Ray, P. R. Nair, and M. A. Alam, “Annealing dependent performance of organic bulk-heterojunction solar cells: A theoretical perspective,” *Sol. Energy Mater. Sol. Cells*, vol. 95, no. 12, pp. 3287–3294, 2011.
- [49] G. Li, Y. Yao, H. Yang, V. Shrotriya, G. Yang, and Y. Yang, “‘Solvent annealing’ effect in polymer solar cells based on poly(3-hexylthiophene) and methanofullerenes,” *Adv. Funct. Mater.*, vol. 17, no. 10, pp. 1636–1644, 2007.
- [50] S. H. Kim, M. J. Misner, T. Xu, M. Kimura, and T. P. Russell, “Highly oriented and ordered arrays from block copolymers via solvent evaporation,” *Adv. Mater.*, vol. 16, no. 3, pp. 226–231, 2004.
- [51] S. Kwon *et al.*, “Effect of Processing Additives on Organic Photovoltaics: Recent Progress and Future Prospects,” *Adv. Energy Mater.*, vol. 7, no. 10, p. 1601496, 2017.

- [52] J. Zhao *et al.*, “Revealing the Effect of Additives with Different Solubility on the Morphology and the Donor Crystalline Structures of Organic Solar Cells,” *ACS Appl. Mater. Interfaces*, vol. 8, no. 28, pp. 18231–18237, 2016.
- [53] M. Heeney *et al.*, “Regioregular poly(3-hexyl)selenophene: a low band gap organic hole transporting polymer,” *Chem. Commun.*, no. 47, p. 5061, 2007.
- [54] Y. Zheng, S. Li, D. Zheng, and J. Yu, “Effects of different polar solvents for solvent vapor annealing treatment on the performance of polymer solar cells,” *Org. Electron. physics, Mater. Appl.*, vol. 15, no. 11, pp. 2647–2653, 2014.
- [55] A. A. B. Alghamdi *et al.*, “Selenophene vs. thiophene in benzothiadiazole-based low energy gap donor-acceptor polymers for photovoltaic applications,” *J. Mater. Chem. A*, vol. 1, no. 16, pp. 5165–5171, 2013.

APPENDIX A



APPENDIX B

For **P1** → 2 mg polymer was dissolved in 4 ml chlorobenzene.

$$\text{mole} = \text{mass} / \text{molecular weight}$$

$$\text{mole} = 2 \times 10^{-3} \text{ g} / 36700 \text{ g mol}^{-1}$$

$$\text{mole} = 5 \times 10^{-8} \text{ mole}$$

$$\text{molarity} = \text{mole} / \text{volume}$$

$$\text{molarity} = 5 \times 10^{-8} \text{ mole} / 4 \times 10^{-3} \text{ L}$$

$$\text{molarity} = 1.25 \times 10^{-5} \text{ mole/L}$$

At 519 nm, P1 shows the maximum absorption. Thus;

$A = \epsilon \times b \times c$ in which ϵ is the molar absorption coefficient, b is the length of the cuvette and c is the concentration

Solution is diluted to 8.3×10^{-7} mole/L.

$$0.790193 = \epsilon \times 1 \text{ cm} \times 8.3 \times 10^{-7} \text{ mole/L}$$

$$\epsilon = 952 \times 10^4 \text{ L mol}^{-1} \text{ cm}^{-1}$$

For **P2** → 1.05 mg polymer was dissolved in 4 ml chlorobenzene.

$$\text{mole} = \text{mass} / \text{molecular weight}$$

$$\text{mole} = 2 \times 10^{-3} \text{ g} / 21000 \text{ g mol}^{-1}$$

$$\text{mole} = 5 \times 10^{-8} \text{ mole}$$

$$\text{molarity} = \text{mole} / \text{volume}$$

$$\text{molarity} = 5 \times 10^{-8} \text{ mole} / 4 \times 10^{-3} \text{ L}$$

$$\text{molarity} = 1.25 \times 10^{-5} \text{ mole/L}$$

At 540 nm, P2 shows the maximum absorption. Thus;

$A = \epsilon \times b \times c$ in which ϵ is the molar absorption coefficient, b is the length of the cuvette and c is the concentration

Solution is diluted to 8.3×10^{-7} mole/L.

$$0.710354 = \epsilon \times 1 \text{ cm} \times 8.3 \times 10^{-7} \text{ mole/L}$$

$$\epsilon = 855 \times 10^4 \text{ Lmol}^{-1}\text{cm}^{-1}$$